GEODESY AND GEODYNAMICS 2015, VOL 6 NO 5, 361–383

Available online at www.sciencedirect.com

ScienceDirect

journal homepage: www.keaipublishing.com/en/journals/geog;
http://www.jgg09.com/jweb_ddcl_en/EN/volumn/home.shtml

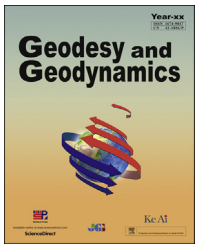

Recent geodynamics of major strike-slip zones

Trifonov Vladimir G.[a,*], *Korzhenkov Andrey M.*[b], *Omar Khaled M.*[b]

[a] *Geological Institute, Russian Academy of Sciences, Moscow, Russia*
[b] *Institute of Physics of the Earth, Russian Academy of Sciences, Moscow, Russia*

ARTICLE INFO

Article history:
Received 16 May 2015
Accepted 4 July 2015
Available online 6 November 2015

Keywords:
Active strike-slip faults
Historical seismicity
Paleoseismicity
Temporal variations of focal mechanisms of earthquakes
Rates of accumulation of strike-slip deformation

ABSTRACT

The subject of this study is strike-slip fault zones, where temporal variations of accumulation in strike-slip deformation complicate the standard process of deformation accumulation and release during strong earthquakes. These temporal variations are expressed in the El Ghab segment of the Dead Sea Transform zone (DST, Eastern Mediterranean) and in the Talas-Fergana fault zone (Central Asia). According to Global Positioning System (GPS) data, the strike-slip deformations within these zones are not now accumulating or are accumulating at a rate that is significantly less than their average rate during the Holocene and Quaternary or the Pliocene–Quaternary. Simultaneously, weak transverse shortening has been measured in both zones by GPS. In both of these zones, strong earthquakes have not registered within the XX century, yet epochs of intensified seismicity (strong earthquakes) took place throughout history. In the southern and central parts of the El Ghab zone, there is evidence of 30 strong historical earthquakes of Ms $\geq$ 5.7; however, no instrumental earthquakes of Ms $\geq$ 5 have been identified. The temporal distribution of seismic energy released by these earthquakes demonstrates a 350 $\pm$ 50-year cycle. Values for the seismic energies released during the peak phases of these cycles are approximated by a sinusoid that suggests the possibility of a $\geq$1800-year cycle ("hyper-cycle"), which began around the 3rd century, reached its maximum in the 12th century, and has continued until now. A combination of geological, archaeoseismological, and geodetic data show that the rate of sinistral strike-slip deformation varied in the fault zone, probably in conformity with the variation of seismicity during the "hyper-cycle." In the Talas-Fergana fault zone, trenching and ^{14}C dating that was correlated with right lateral offsets, gave a possible preliminary estimate of the average rates of the Late Holocene strike slip of about 10 mm per year, with a decrease in the SE direction to 4 mm–4.5 mm per year. These studies also showed that the slip in the Talas-Fergana fault zone was realized mainly during strong earthquakes. New trenching and ^{14}C dating of paleoearthquake records identified the epoch of seismicity intensification dating to the XIV–XVII centuries. These paleoearthquakes could produce a total dextral slip at several meters. Therefore, consideration of these epochs was necessary to determine a calculated average slip rate during the Late Holocene.

The main shock and the strongest aftershocks of the Altai earthquake of September 27, 2003, with Ms = 7.0 demonstrated a strike-slip focal mechanism with an NW-trending

* *Corresponding author*. Tel.: +7 916 5404052; fax: +7 495 9510443.
E-mail address: trifonov@ginras.ru (Trifonov V.G.).
Peer review under responsibility of Institute of Seismology, China Earthquake Administration.

Production and Hosting by Elsevier on behalf of KeAi

http://dx.doi.org/10.1016/j.geog.2015.06.003

plane of the right lateral slip. An approximately 65 km-long NW-trending seismic rupture with a right lateral slip of up to 2 m, formed during the earthquake. The aftershock activity significantly decreased in 2004–2005 when reverse and rarer normal focal mechanisms became dominant. In the Palmyrides and the southern Aleppo block (NW Syria), strong earthquakes in 1994 (Mw = 5.3) and 1996 (Mw = 5.5) had strike-slip focal mechanisms, while only weak (magnitudes 1.1 to 3.3) earthquakes occurred in 2009–2011; the overwhelming majority of these weak earthquakes had normal and reverse mechanisms.

In all of the cases mentioned above, strike-slip deformation was expressed only or mainly during strong earthquakes. At other times, the rate of its accumulation was small and the dominant stress conditions led to transverse shortening, rarely resulting in local lengthening of the tectonic zone. These variations are caused by the tectonic peculiarities of these zones. The sinistral component of the deformation is related to the shift of the Arabian Plate relative to the African one, but also the transverse component is related to the continental slope and is expressed by the Coastal range shortening that exists in the El Ghab segment zone. There is not only a dextral deformation component, but also a transverse component, expressed by shortening of the Fergana and Talas ranges existing in the Talas-Fergana fault zone. In both zones, the shortening component became appreciable or dominant when the strike-slip deformation rate decreased. Similar, but more local, relationships were expressed in the epicentral area of the 2003 Altai earthquake and in the Western Palmyrides.

1. Introduction

Recent geodynamics of major strike-slip faults in orogenic regions can be studied using three groups of methods. The first group consists of geological and geomorphological studies of young strike-slip offsets and the associated deformation of topographic features, geological bodies, and archaeological objects. The second group focuses on the identification and parameterization of instrumental and historical earthquakes, as well as expressions of archaeoseismicity and paleoseismicity. Estimation of offset ages is the most difficult part of determining the average rate of Late Quaternary displacement on strike-slip faults. The same difficulty exists for the estimation of past earthquake dates if instrumental and historical data are absent. In this situation, we determine the age of objects that were deformed during the earthquake or that were formed as the result of the earthquake, or later. These objects provide the upper and lower limits for the earthquake age. An attempt to estimate the age of an event by dating of the colluvial wedge is often erroneous, because the analyzed material of the wedge (for example, the lower layer of the displaced soil or the earlier archaeological artifacts) can be older than the wedge itself. A wide set of methods must be used for this type of dating and the resultant precision is not usually better than several decades. A combination of the methods (for example, use of both the historical chronicles as well as the archaeoseismology and paleoseismology data) offers the most reliable estimation of pre-instrumental earthquake parameters.

The third group combines the results of the repeated geodetic, especially Global Positioning System (GPS), observations. There are three movements regimes on active faults. They are: (1) creep, accompanied by weak earthquakes; (2) a combination of creep and rare strong earthquakes; and (3) displacements, only during rare strong earthquakes. Regimes (1) and (3) are rarely realized, while different variants of regime (2) have the most wide-spread usage. According to regime (2), elastic deformation is only partly released during creep time intervals and is gradually accumulated, leading from time to time (often periodically) to strong seismic releases of accumulated deformation resulting in significant displacement on the fault. If the GPS observations record the entire fault zone, they can register the total accumulated deformation that is expressed in the land surface and the results do not depend on whether the deformation is realized by immediate offset and permanent deformation or if it exists elastically for the time being.

If the deformation accumulates permanently, the rates of deformation, estimated using different methods, must be approximately the same, although they characterize different time intervals. The rate of the geological deformation is estimated by the average rate of the displacement on the fault during some time interval. The seismological estimate is a sum of the seismic displacements during the fixed time interval with corrections for the contributions of creep and weak earthquakes. The geodetic (GPS) estimate expresses the total accumulated deformation, but is related to the shortest time interval, usually not more than one decade, but can rarely be several decades.

The estimations of the lateral slip rates, obtained using different methods, are similar to those of major interplate strike-slip faults, such as the San Andreas Fault in California and the North Anatolian Fault in Turkey. This shows that strain release rates on those faults result in more or less permanent average slip rates. Molnar and Dayem [1] summed

data and argued this conclusion for the San Andreas right lateral fault zone. On the North Anatolian right lateral fault zone, the average Quaternary dextral slip rates were estimated at 18 mm/a to 20 mm/a in the eastern part of the zone and at 13 mm/a in the central part using offsets of major river valleys [2]. The Late Holocene rates of 20.5 ± 5.5 mm/a and 18.6 ± 3.5 mm/a were measured in the central part of the zone [3,4]. In the western region, the fault splays into separate strands and Pucci et al. [5] measured an average slip rate of 15.0 ± 3.2 mm/a for the northern strand over the past 60,000 years. Kiratzi [6] calculated the rate of slip using tensors of seismic moments of XX-century earthquakes. The slip rate was found to decrease from 27 mm/a in the east to 16 mm/a in the west. The summing lateral slip of 5 m–8 m during the last seismic cycle, reaching a maximum in the Dec.26 1939 earthquake with Ms = 7.8, was divided in the approximately 300-year duration of the cycle, and gives an average rate of 17 mm/a to 27 mm/a [7]. The rate of accumulation of the recent strike slip, obtained in the 1990s by GPS measurements is estimated at 26 mm/a [8]. Later GPS measurements and calculations [9] showed that the rate of the deformation accumulation is approximately 24 mm/a, which is dispersed in the 100-km wide belt and only approximately 20 mm/a (≤15 mm/a in the central part) is concentrated in the fault zone itself. Re-calculation for the balanced block model gave strike slip rates from 25.7 ± 0.2 mm/a in the eastern part of the zone and up to 24.2 ± 0.2 mm/a in the western part [10].

The deformation can be released on different segments for both mentioned zones, either by creep and relatively weak earthquakes or by displacements during one or several earthquakes at active phases that are separated by stages of relative seismic quietness. The means of deformation release depends on the mechanical properties of the rocks. This peculiarity is described and argued in detail for the San Andreas [11–13] and North Anatolian [7,14] fault zones.

New data have been obtained for the Eastern Mediterranean and for Central Asia during recent years. This data shows that the rate of elastic deformation accumulation has varied, there is less in these strike-slip zones now than there has been during the phases of seismic activity. These zones are analyzed in the present paper.

2. The El Ghab segment of the Dead Sea Transform in Eastern Mediterranean

The Dead Sea Transform (DST), named also as the Levant fault zone, forms the western boundary of the Arabian Plate. This zone reveals attributes of Late Quaternary left-lateral strike-slip offsets with a subordinate vertical component and consists of several strands in its northern part. The main strands are the Yamounneh Fault in Lebanon and the El Ghab Fault in Western Syria and Southern Turkey (Fig. 1). The El Ghab Fault includes the pull-apart Basin of the same name and, in the north, it is conjugate with the southwestern termination of the active East Anatolian fault zone (EAFZ), which is characterized by left-lateral–reverse strike-slip offsets.

The estimation of the average rate of the Quaternary movements on the Yamounneh Fault is based on the 4 km-offset of the Litani River valley [15]. Westaway [16] dates the beginning of the regional humidification and incision epoch at approximately 870,000 years, which gives an average strike-slip rate of approximately 5 mm/a. The estimation of the Holocene strike slip was obtained on the eastern slope of the Lebanon Ridge from the offset of the Zalka alluvium fan (approximately N33°50′). The old fan generation is offset at 56 ± 5 m and its surface was dated, using the ^{36}Cl technique, at 11.20 ± 0.81 thousand years [17,18]. This gives the average slip rate of 3.9 mm/a to 6.1 mm/a. Trenching in the small fault basin near the village of Yamounneh showed that the Holocene offset is the cumulative effect of several strong earthquakes. According to GPS measurements, the accumulation rate of the contemporary elastic deformation corresponds to 4.8 ± 0.4 mm/a of strike slip [10] or to 4 mm/a to 5 mm/a of strike slip with a subordinate component of transverse shortening [19].

In the more southern, Jordan segment of the DST (Gor-Qatar locality in the left bank of the Jordan River), the maximum sinistral offset has reached 240 ± 20 m during the last 47.5 thousand years, giving an average rate of strike slip of 4.9 mm/a [20]. A more detailed study of the quoted authors showed that shifts during strong earthquakes contributed the main portion to the offset and the average rate varied from 4.5 mm/a to 5.3 mm/a 7–9 thousand years ago and decreased later to 3.4 mm/a. The accumulation rate of the contemporary elastic deformation is estimated from GPS data as 4.4 ± 0.3 mm/a [10].

The estimations of the strike-slip rates, obtained in both considered segments of the DST by different techniques and characterized over different time intervals, are similar.

Other relationships have been found in the El Ghab segment. This segment of the DST formed in the Pliocene, 4 Ma to 3.5 Ma [21,22]. The average rate of Pliocene-Quaternary sinistral slip has been estimated in two ways. Chorowicz et al. [23] and Gomez et al. [24] correlated elements of the Late Miocene–Early Pliocene volcanic structure from both sides of the fault: they are offset 16 km–20 km to the left. The other way of estimation is based on the correlation of the ophiolite sections of the Bassith zone to the west of the El Ghab segment and the Kurd Dagh zone to the east. The Bassith zone is bounded to the SE by the Lattaqieh Fault, and the Kurd Dagh zone is bounded to the SE by the Aafrin Fault. Both boundary faults, as well as the ophiolite nappes, strike to the NE obliquely to the El Ghab fault zone, which is approximately 20 km wide. This produces some uncertainty in the estimate of the slip magnitude, which cannot be determined more accurately than as16 km to 20 km [22]. The 16 km–20 km offset during 4 Ma to 3.5 Ma gives yields an average slip rate of 5 ± 1 mm/a.

The same average rate has been determined by analysis of the Holocene sinistral offsets in the 26-km long segment of the southern part of the El Ghab zone, between the villages of Sahlieh in the north and Al Baida in the south [22,25]. There, the fault zone is less than 1 km wide and consists of several strands, which are arranged en echelon to each other and form a very sharp angle with the zone axis. In cross-sections of the zone there are usually two main distinguishable faults crossing valleys of small rivers and ravines of different length and development, suggesting their different age. The valleys

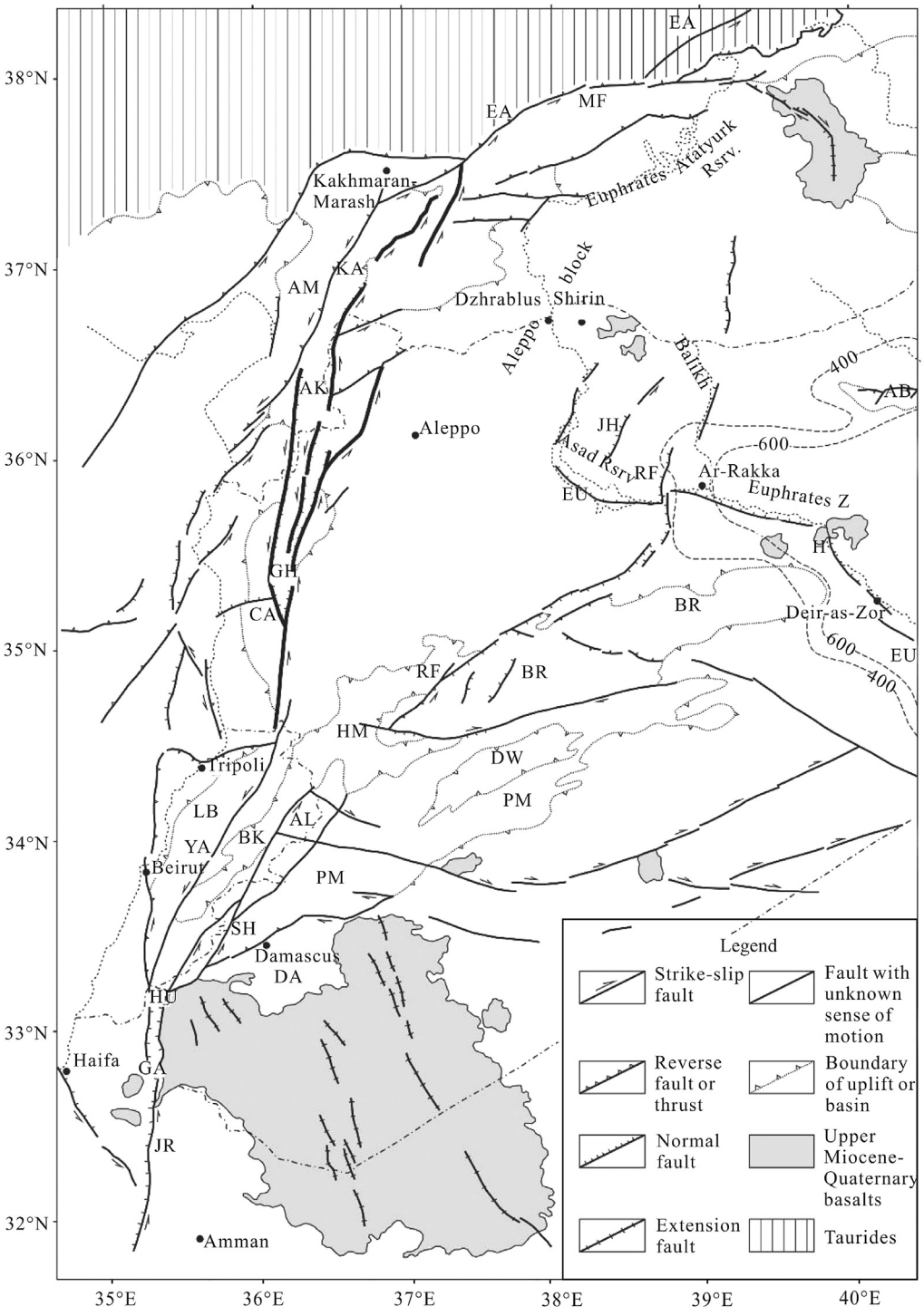

Fig. 1 – Late Pliocene–Quaternary epoch (last about 3.5 Ma) tectonic elements of the North-Western Arabian Plate. In Fig. 1, the El Ghab fault zone is indicated by the thickened lines. The 400-m and 600-m Miocene isopachs and the 500-m Pliocene isopach demonstrate the structure of the Mesopotamian Foredeep [26]. Anticlines and uplift zones: AB, Abdel Aziz; AL, Anti-Lebanon; BR, Bishri, Northern Palmyrides; CA, Coastal range of Syria; LB, Lebanon range; MF, Marginal Folds of Turkey; and PM, Southern Palmyrides. Faults and fault zones: Am, Amanos, EAFZ segment; EA, EAFZ; EU, Euphrates; JA, Jhar; JH, Beer Jabel–Heimer Kabir; JR, Jordan segment of DST; OL, Olab; RF, Rasafeh–El Faid; SH, Serghaya; and YA, Yammuneh segment of DST. Basins: AK, Amik; BK, Bekaa Syncline; DA, Damascus; DW, Ad Daw; GA, Sea of Galilee pull-apart Basin, DST; GH, El Ghab pull-apart Basin, DST; HM, Homs Basin; Hu, Hula pull apart Basin, DST; and KA, Karasu Graben. Basaltic fields: H, Halabieh; and Z, Zalabieh.

and their elements (channels, slopes, and terraces) of different age are offset to the left at different distances. In the north, the 30 m–40 m offsets on the western strand and the 13 m–20 m offsets on the eastern strand are related to the shortest valleys and recent channels, and are dated to the Holocene. In the south, near Al Beida, the offset on the western strand decreases down to 25 m and only a part of it can be attributed to the Holocene. However, on the eastern strand, the Holocene landforms are offset at 34 m–40 m. So, from the north to south, the offset on the western strands decrease and those on the eastern strands increase, but the total Holocene offset continues to be approximately 50 m, giving an average slip rate of approximately 5 mm/a. Thus, the 5 ± 1 mm/a rate is a rather permanent parameter for both the Pliocene–Quaternary and Holocene movements.

The sinistral offset of the Roman aqueduct in the southern part of the El Ghab zone near the village of Al Harif allows an estimation of the strike-slip rate during a shorter time interval. The aqueduct is offset at approximately 12 m [21,22] or 13.6 ± 0.2 m, if one adds a bend of the aqueduct near the fault that Meghraoui et al. [27] considered to be tectonic. The aqueduct was built in the I century BC to I century AD, but not earlier than 63 BC [27,28]. Therefore, the average rate of its displacement is 6 mm/a to 6.8 mm/a. Trenching in the fault zone showed that this offset was the cumulative effect of a minimum of three strong earthquakes, the latest of which, the 29.06.1170 earthquake, being the strongest [27]. The shift during that earthquake could have been 4 m–4.5 m (a third part of the total offset), or more. Taking into account that the intensity of the 1170 shock reached IX–X of the Medvedev-Shebalin-Karnik (MSK) scale in the Southern El Ghab zone and that the VIII isoseismal occupied a approximately 170-km long segment of the DST (Fig. 2), we estimated the earthquake magnitude as Ms = 7.8 and located its epicenter near the aqueduct or a little southward [22]. We compared our preliminary estimation of the 1170 earthquake offset with the data of Wells and Coppersmith [29]. Using their equations, we calculated an average displacement (AD) of 5 (4–6) m and a maximum displacement (MD) of 10 (7–12) m for earthquakes with moment magnitude M = 7.8.

Five sessions of GPS measurements were carried out in 2005–2008 around the southern and central parts of the El Ghab zone by the Joint Russian-Syrian Group. The GPS equipment included four Leica GKL 122 chargers, five GEB71 NICd 700 mA/14 h batteries, and several batteries of lower capacity. Satellite signals were registered at L1 and L2 frequencies with a 30 s update rate and a 10° cutoff angle. The data were processed using the standard Leica SKI PRO software, as applied to WGS-84 ellipsoid. An analysis of the data, obtained in 2004, using the chosen measurement procedure and using date processing showed that the errors in the horizontal, vertical, and spatial positioning did not exceed 1 mm, 4.5 mm, and 4.6 mm, respectively; GORS was chosen as the reference point. This technique was used for the corresponding 2005–2008 GPS measurements in the quadrangles "Missyaf" and "El Ghab" around the southern and central parts of the El Ghab fault zone (Fig. 3). The changes in distances

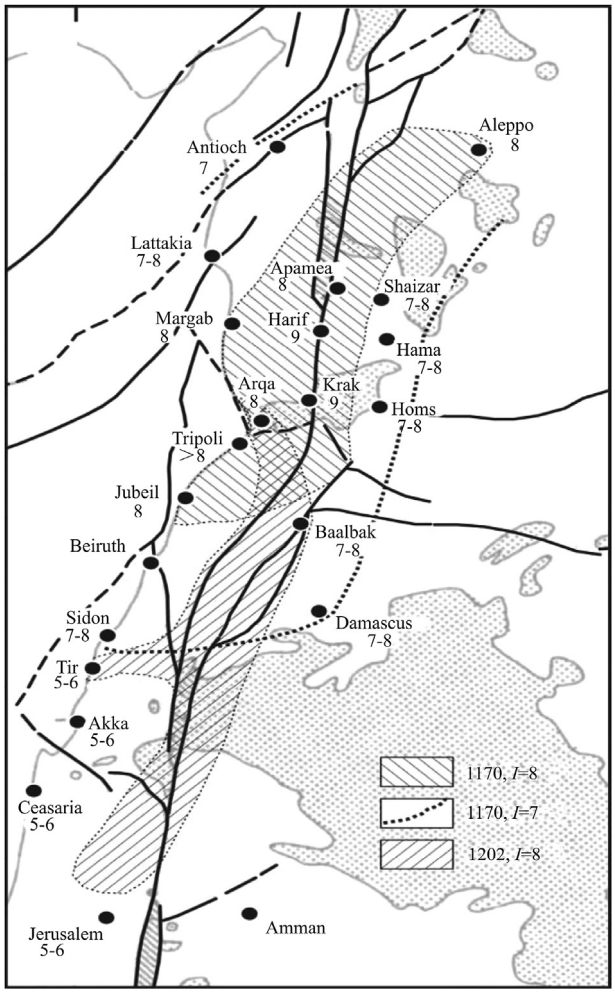

Fig. 2 – Map of isoseists of the 29.06.1170 earthquake [22] compared with isoseist 8 of the 20.05.1202 earthquake [30].

between the points of the quadrangles (Tables 1 and 2) can be interpreted as a 1 mm/a sinistral slip rate, combined with the transverse shortening component on the southern part of the El Ghab zone and a transverse shortening of ≤1 mm/a without strike slip on the central part [23,31]. Analogous GPS measurements were carried out around the El Ghab zone in other network in 2000, 2007, and 2008 by the American-Syrian Working Group. These studies showed an accumulation of deformation corresponding to a sinistral slip rate of 1 mm/a to 2 mm/a [32,33]. Thus, two independent studies proved that the contemporary sinistral slip rate is 2–5 times less than the long-term average strike-slip rate. At the same time, the contemporary transverse shortening rate reaches approximately 1 mm/a, and is commensurable with the strike slip.

We have compared the estimated rates of motion on the El Ghab zone with seismicity changes from data for instrumental-recorded and historical earthquakes, archaeoseismology, and paleoseismology, using values of seismic

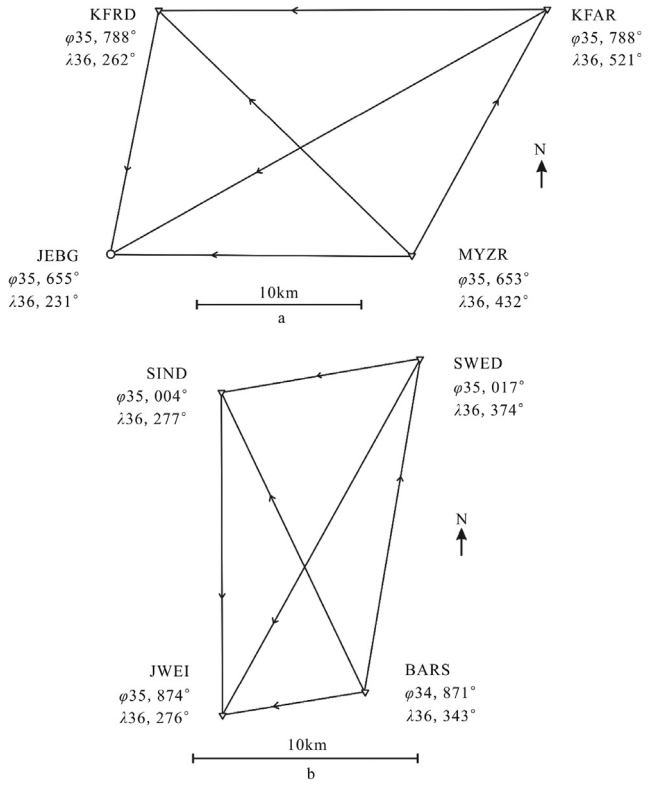

Fig. 3 – GPS measurement points within the El Ghab fault zone: (a) the El Ghab quadrangle in the central part and (b) the Missyaf quadrangle in the southern part.

energy released by earthquakes during the century as a criterion [22,26]. To estimate the value of the released seismic energy, we used the F.T. Aptikaev's equation, which links energy E (J.) and magnitude Ms:

$$E = 10^{[8.1+0.9098(M+1.55)]}$$

We have excluded the northern part of the El Ghab zone from consideration, due to the uncertainty in the identification of its epicenter locations, or whether some of the earthquakes belong to the northern El Ghab zone or the EAFZ. In the southern and central El Ghab zone (between N34.5° and N36.15°), 30 historical earthquakes of Ms ≥ 5.7 and no instrumentally-recorded earthquakes from the XX century of Ms ≥ 5.0 have been registered from the beginning of the I century AD (Table 3).

Analyzing the temporal distribution of the released seismic energy values, we find that strong earthquakes occurred with periodicity 350 ± 50 years (Fig. 4a). This recurrence may be a manifestation of seismic cycles, in terms of Fedotov [34]. At the same time, the values of energy released at the maximum phases of these cycles changed from cycle to cycle: it was moderate in the I century, decreased in the V century, and later increased, reaching a maximum, in the XII century. The value of the released energy decreased, but remained high, in the maximal XV-century phase of the next cycle and then sharply diminished, to the complete absence of the earthquakes of Ms ≥ 5.0 in the XX century. So, a longer cycle ("hyper-cycle"), with a period of ≥1800 years, has been identified that encapsulates 350 ± 50-year cycles. The "hyper-cycle" began in the III century, reached its maximum in the XII century, and continued, minimally, up to the beginning of the XXI century.

It is possible to explain the temporal variations of the accumulation rates of deformation in the El Ghab fault zone, assuming that the rates varied in proportion to the value of the released seismic energy. The recent epoch is characterized by low seismicity and, correspondingly, to a low rate of accumulation of strike-slip deformation. The rate is a little

Table 1 – Changes in distance (D) between the points of the Missyaf quadrangle in the southern part of the El Ghab fault zone, according to results of the 2005–2008 GPS measurements [23].

REF point	ROV point	Distance between the points (m) in					Distance change between 11.2005 and 06.2008 (mm)
		11.2005	05.2006	10.2006	04.2007	06.2008	
BARS	JWEI	6423.9255	6423.9271	6423.9277	6423.9280	6423.9283	+2.8
BARS	SIND	14,922.2185	14,922.2171	14,922.2169	14,922.2166	14,922.2168	−1.7
BARS	SWED	15,215.8301	15,215.8297	15,215.8291	15,215.8288	15,215.8286	−1.5
SWED	JWEI	18,304.3772	18,304.3753	18,304.3749	18,304.3745	18,304.3748	−2.4
SWED	SIND	9094.2677	9094.2651	9094.2647	9094.2642	9094.2645	−3.2
SIND	JWEI	14,484.0797	14,484.0781	14,484.0779	14,484.0775	14,484.0778	−1.9

Table 2 – Changes in distance (D) between the points of the El Ghab quadrangle in the central part of the El Ghab fault zone, according to results of the 2005–2008 GPS measurements [23].

REF point	ROV point	Distance between the points (m) in					Distance change between 11.2005 and 06.2008 (mm)
		11.2005	05.2006	10.2006	04.2007	06.2008	
JEBG	KAFR	15,028.7617	15,028.7591	15,028.7586	15,028.7582	15,028.7586	−3.1
JEBG	KFRD	30,220.9128	30,220.9101	30,220.9099	30,220.9095	30,220.9098	−3.0
JEBG	MZWR	18,245.8299	18,245.8266	18,245.8261	18,245.8258	18,245.8259	−4.0
MZWR	KAFR	21,414.0415	21,414.0421	21,414.0424	21,414.0428	21,414.0431	+1.6
MZWR	KFRD	17,010.8116	17,010.8133	17,010.8139	17,010.8142	17,010.8145	+2.9
KFRD	KAFR	23,478.4970	23,478.4950	23,478.4947	23,478.4943	23,478.4949	−2.1

Table 3 – Catalogue of historical earthquakes of magnitudes Ms ≥ 5.7 in the southern and central sub-segments of the El Ghab Fault Zone, Syria.

No.	Year	Month	Day	Reference	φ	λ	Ms	I_0	H
1.	37	–	–	[35]	36.0	36.3	6.2	7–8	15
2.	47–48	–	–	[36]	35.7	36.3	6.7	7	20
3.	53	–	–	[37,38]	36.2	36.5	7.0	8	30
4.	458	9	14	[36,38–40]	36.2	36.4	7.7	9	20
5.	477			[35]	35.3	35.9	5.7		
6.	494	–	–	[38,40]	35.8	36.3	6.6	8	25
7.	557	10	19	[38,39]	36.1	35.55	6.0	–	–
8.	565–571	–	–	[38,39]	36.0	36.2	6.0	7–8	30
9.	713	2	28	[37,38,41–43]	35.7	36.3	7.0	9	–
10.	860	1		[36,38,39]	35.7	36.4	7.4	9–10	33
11.	1091	9/10	26/06	[38,39]	36.35	36.10	7.4	9	–
12.	1094	4–5	–	[38,40,44]	35.90	36.30	6.0	6	–
13.	1157	4	02/04	[38]	35.50	36.50	6.0	7	22
14.	1157	7	13	[38,42,45]	35.20	36.60	6.6	8	25
15.	1157	8	12	[25,38,42,46,47]	35.40	36.50	7.4	9–10	15
16.	1170	6	29	[25,27,37,38,40–42,46]	35.0	36.30	7.7	9–10	35
17.	1183–1190	9	–	[39]	36.00	36.30	6.1	–	–
18.	1290–1292			[38,40]	35.15	36.73	6.8	8	–
19.	1404	2	20	[37,38,42]	35.70	36.20	7.4	9	30
20.	1404	11–12		[37,38,42]	35.70	36.20	5.7	6	
21.	1407	4–5	–	[38,39,42,46–48]	35.7	36.4	7.0	10	–
22.	1408	12	29	[37,38,42,48]	35.80	36.10	7.4	9–10	25
23.	1537	1	07	[38,39,43]	35.8	36.3	6.4		20
24.	1577	1	28	[38,42,43]	35.50	36.50	6.6	–	–
25.	1656	2		[35,38,42,45]	34.60	36.40	6.6	8–10	–
26.	1765			[35,42,49]	34.50	36.35	6.4	–	–
27.	1783	7	20	[35,42,43]	35.6	36.40	6.5	–	–
28.	1796	4	26	[38,40,42,47,49]	35.30	36.30	6.8	8–9	20
29.	1822	8	13	[37,38,42,45,50,51]	36.10	36.75	7.0	9	18
30.	1822	9	05	[37,38]	36.10	36.75	5.7	7	

φ, λ–latitude and longitude of epicenter; Ms–magnitude Ms; I_0–intensity in epicenter; H–depth of hypocenter.

higher during the past two millennia than the average slip rate, as this time interval occupied not only the whole last hyper-cycle, but also the end of previous one, when the seismicity was relatively high in the I century AD.

3. The Talas-Fergana Fault in Tian Shan

The NW-trending active Talas-Fergana dextral Fault cuts the Tian Shan mountain system, which was formed in the Paleozoic orogen and was reworked into a peneplain in the Early Paleogene. Now, the Tian Shan represents the marginal deformation zone of the Eurasian Plate in its boundary with the Alpine-Himalayan collisional belt (Fig. 5). The Talas-Fergana Fault is expressed in topography by scarps and numerous dextral offsets of intersected valleys, watersheds, and other topographic features along the whole 500-km crossing of Tian Shan, between the western Kokshaal range in the SE and the intermountain Upper Talas Basin near the northwestern termination of the Talas range. The fault is vertical or dips very steeply beneath the southwestern uplifted side. Farther to the NW and SE, the fault is traced fragmentally and is also characterized by strike-slip offsets, but these are essentially smaller. The total fault length reaches approximately 900 km.

Burtman [52] showed that the total dextral offset on the fault can reach approximately 200 km. The total Quaternary strike slip during the last approximately 1.8 Ma is estimated at 12 km–14 km by the correlation of major topographical features in the fault sides [53]. This gives a 6.5 mm/a to 8 mm/a average strike-slip rate. Pleistocene offsets have been found in glacial deposits and topographical features. For example, the lateral moraine of the Late Pleistocene valley glacier is offset at 135 m–150 m in the right bank of the Keklikbel River (Fig. 6; the location is shown in Fig. 7). Preservation and features of the moraine are characteristic of the Late Pleistocene glacial forms [54] and are correlated with the Valdaian Glaciation in Russia, the Middle Weichselian in NW Europe, and the Wisconsinan Glaciation in North America, and dating back to approximately 75 to 11 thousand years (www.stratigrahy.org). This permits a lower-limit estimation of the strike-slip rate at 2 mm/a to 15 mm/a. Near the same site [53] and in the upper Karasu River [55], the moraines and trough valleys of the late Middle Pleistocene age are offset to the right at 700 m–800 m (Fig. 8). These glacial features can be correlated with the Moscovian glaciation in Russia, the Late Saalian in NW Europe, and the Illinoian glaciation in North America, and dating back to approximately 130–180 thousand years ([54]; www.stratigrahy.org). This gives a possible lower-limit estimation of the average strike-slip rate of 4 mm/a to 6 mm/a. Also, the vertical component is 10–30 times smaller. To the NW of the Toktogul Reservoir, the upper Janaryksay River valley shows signs of trough structure and

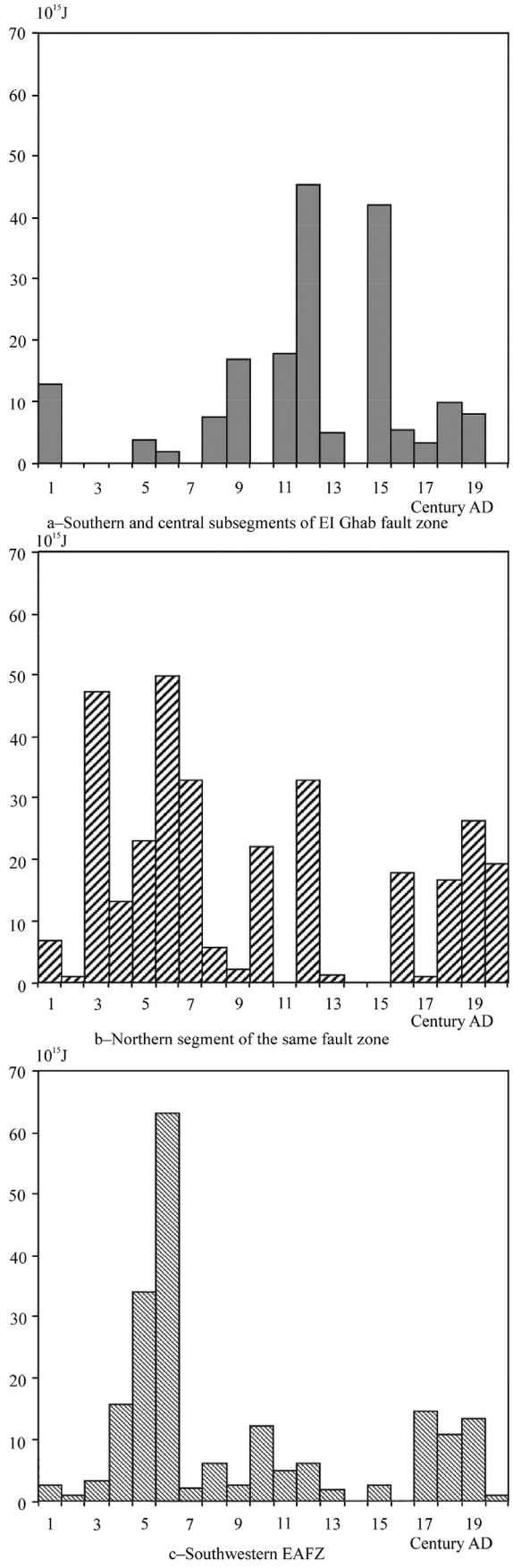

Fig. 4 – Bar charts of the time-dependent distribution of 100-year seismic energy released by earthquakes of magnitudes Ms ≥ 5.7.

relics of a lateral moraine that are possibly from the same glaciation, which are offset to the right at 1500 m. This corresponds to a lower limit strike-slip rate of 8 mm/a to 12 mm/a.

The Late Holocene dextral offsets were studied in detail in the 350-km part of the fault (Fig. 9). To estimate slip rates, we studied the sections of small near-fault basins that were formed by damming valleys by their offset sides and/or by contrary scarps simultaneous to lateral displacements. The age of basal deposits in the basin section gives the upper limit of the displacement age. Much more rarely, we could estimate the lower limit of the age of lateral displacement by dating offset topographical features. All collected samples were dated by the ^{14}C technique and calibrated.

The study region was divided to six segments. The south-eastern segment I begins 60 km from the Chinese-Kyrgyz boundary and extends 20 km from the Kockiya Pass, up to the Jilangach River (Figs. 7 and 10). The age of the deposits in this small basin correlated with the 19-m lateral offset is 3970 ± 40 years (calibrated 2580 to 2340 BC with a probability of 95.4%) (I-1 in Fig. 10) that gives an upper limit for the average slip rate of 4.1 mm/a to 4.4 mm/a [53]. Burtman et al. [56] reported a 40 ± 3-m offset and an accompanying former sag pond with a calibrated age of 2777 BP to 2934 BP in the NW area of the segment, near Jilangach Pass between the Jilangach and Biruzy rivers (I-2 in Fig. 10). This determines an upper limit of the average slip rate as 13 mm/a to 15 mm/a. Since the dated sample was collected 22–30 cm above the base of the 1-m section, the sag pond could have be formed earlier and, correspondingly, the upper limit of the slip rate might be reduced to 9 mm/a to 11 mm/a.

The 30-km long segment II cuts through the basins of the Pychan and Kyldou rivers. In the SE area of the segment, the calibrated age of the lower deposits in the basin accompanying the 35 ± 5-m offset is 3070 BP to 3360 BP (II-3 in Fig. 10) [56], and the age of the deposits accompanying the 27 ± 1-m offset is 3740 ± 600 years (calibrated 3100 BC to 1400 BC with a probability of 68.2%) (II-4 in Fig. 10) [53]. This data give an upper limits to the average slip rates of 9 mm/a to 13 mm/a and 5.1 mm/a to 8.3 mm/a, correspondingly. Farther to the NW, Burtman et al. [56] reported an offset of 21 m–24 m and the calibrated age of the lower deposits in the accompanying former sag pond to be 2540 BP to 2752 BP (II-5 in Fig. 10), which gives an upper limit of the average slip rate of 8 mm/a to 9 mm/a. Trifonov et al. [53] reported a 23 m to 24-m offset in the Kyldow River and the accompanying sag pond deposits to have an age of 2320 ± 40 years (calibrated 520 BC to 350 BC with a probability of 78.3%) (II-6 in Fig. 10) that corresponds to an upper limit slip rate of 9.2 mm/a to 10.3 mm/a.

The 35 km-long segment III extends from the Kongurtobe River up to the Kuroves River. The paleosoil in a terrace-like surface is offset to 17 m–20 m, and is dated to 1510 ± 60 years (calibrated 420 AD to 650 AD with a probability of 95.4%) (III-7 in Fig. 10), which gives a lower limit slip rate of approximately

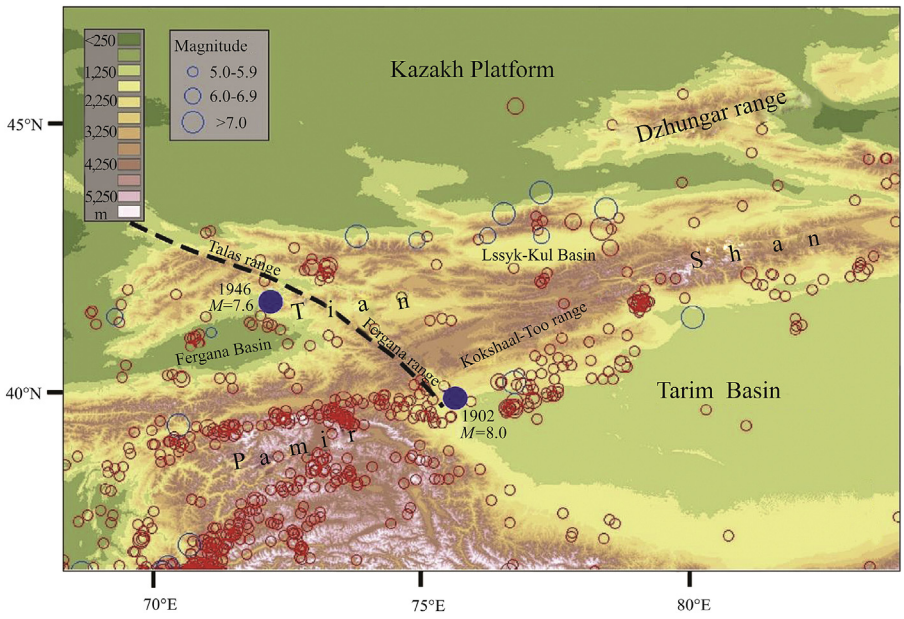

Fig. 5 – Position of the Talas-Fergana Fault in Central Asia and the epicenters of instrumentally-recorded (brown circles) and historical (green circles) earthquakes [57].

10 mm/a to 15 mm/a [53]. The 25-km long segment IV crosses the basins of the Kuroves and Keklikbel rivers. The basal deposits of the small basin, perhaps, accompanying the 10-m to 12-m lateral offset, are dated to 1240 ± 60 years (calibrated 660 AD to 900 AD with a probability of 93.4%) (IV-8 in Fig. 10) that corresponds to an upper limit slip rate of 7.3 mm/a to 11 mm/a.

The 60-km long segment V strikes along the upper Karasu River and farther along via the Kokbel Pass and up to the Toktogul Reservoir in the Naryn River. Paleosoils of calibrated ages from 2340 ± 120 years (calibrated 800 BC to 100 BC with a probability of 95.4%) to 4900 ± 230 years (calibrated 4300 BC to 3000 BC with a probability of 95.4%) were found in dry valley sections near the Kokbel Pass (V-9 in Fig. 10) [58,59]. Perhaps, these dates characterize the age of the offset landforms. The most characteristic strike-slip offsets of the dry valleys are 17 m–18 m and 35 m–38 m [53]. Comparison of these data yields a estimation of the lower limit for the strike-slip rate of 5.5 mm/a to 8.6 mm/a.

The 180 km-long segment VI extends from the Toktogul Reservoir up to the northwestern slope of the Talas range, crossing the Janaryksai, Ustasai, and Karakulja rivers, and the sources of the Atoinok and Chatkal rivers. In the Janaryksai, Burtman et al. [56] reported a 14 ± 2-m offset and dated the

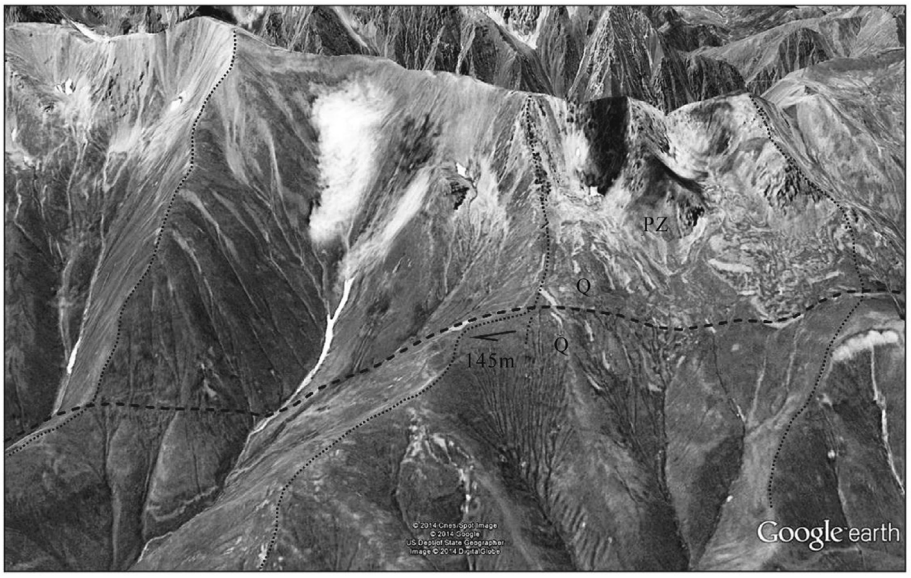

Fig. 6 – The dextral offset of the Late Pleistocene lateral moraine on the Talas-Fergana Fault in the right bank of the Keklikbel River. The location is shown in Fig. 7.

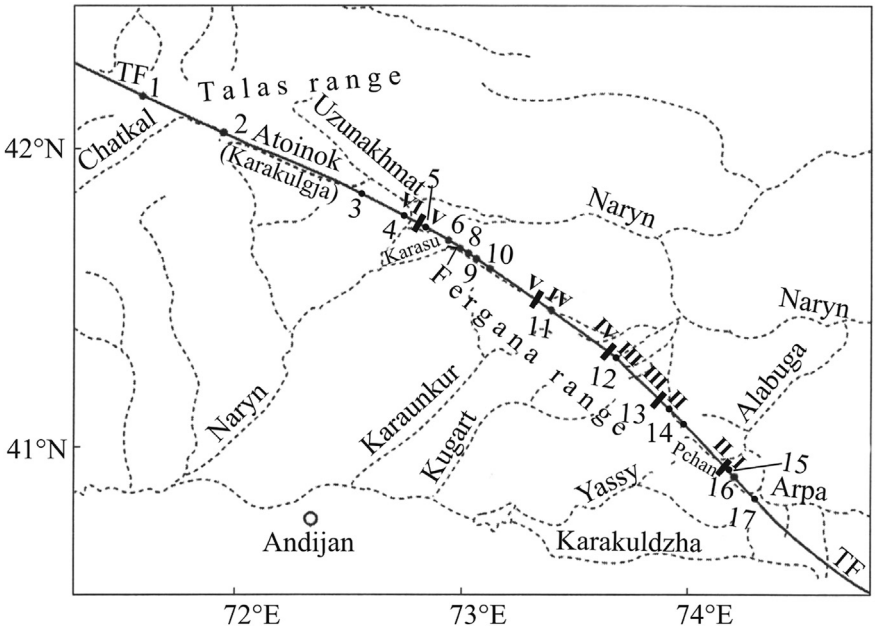

Fig. 7 – Talas-Fergana Fault in slopes of the Talas and Fergana ranges. Geographic names, mentioned in the text: (1) Karabura Pass; (2) Karakuldzha Pass; (3) Ustasai; (4) Djanaryksai; (5) Toktogul Reservoir; (6) Kokbel Pass; (7) Karasu-1 site; (8) Karasu-2 site; (9) Karasu-3 site; (10) rockfall-generated lakes in the upper Karasu River; (11) Keklikbel River; (12) Kuroves River; (13) Kongurtyube River; (14) Kyldow River; (15) Biruzy River; (16) Jilangach River; and (17) Kockiya Pass. The fault segments I–VI are shown.

accompanying sad pond deposits to 1311 BP to 1361 BP (VI-10 in Fig. 10), giving an upper limit average slip rate of 9 mm/a to 12 mm/a. Burtman et al. [60] reported data to estimate average strike-slip rates for the Atoinok River source and the upper Chatkal River. Peat and paleosoil, 1450 ± 40 years (calibrated 540 AD to 660 AD with a probability of 95.4%) (VI-11 in Fig. 10), fill in the small basins that accompany the 17-m to 20 m strike-slip offsets. This gives an upper limit strike-slip rate of 12 mm/a to 15 mm/a. An offset of 20 m and an age of sag pond deposits of 1928 BP to 2030 BP (VI-12 in Fig. 10) were reported by Burtman et al. [56], and give an upper limit slip rate of approximately 10 mm/a.

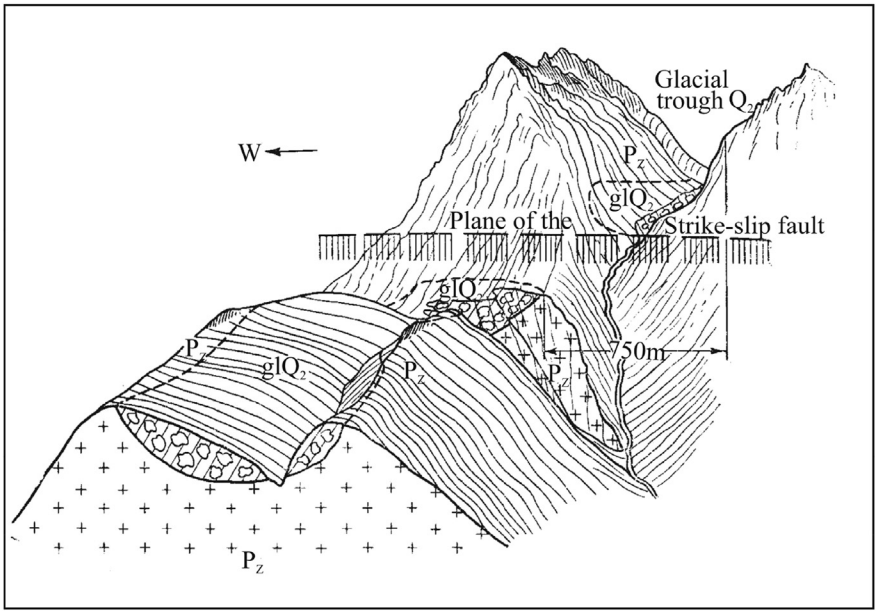

Fig. 8 – The dextral offset of the late Middle Pleistocene glacial trough on the Talas-Fergana Fault in the upper Karasu River valley [55].

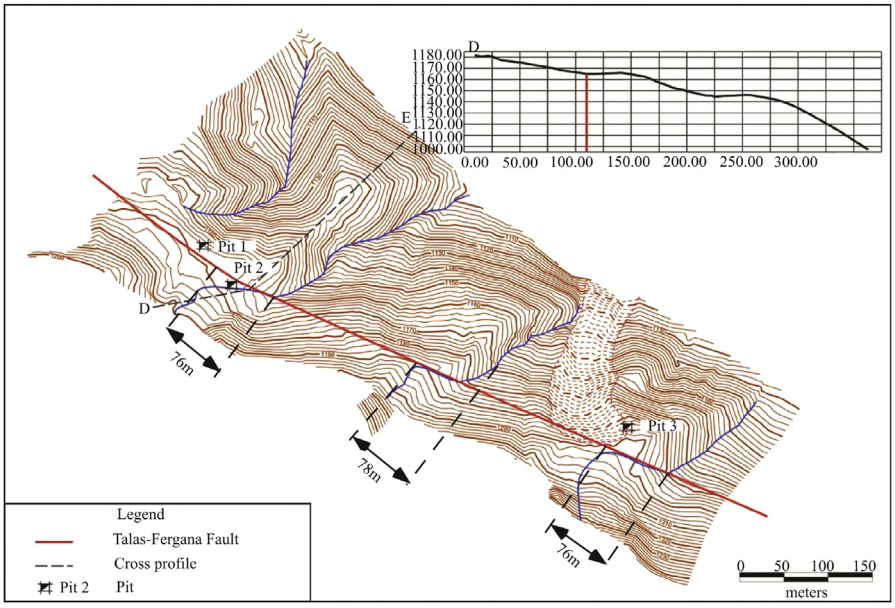

Fig. 9 – The dextral offsets of the Holocene landforms on the Talas-Fergana Fault near the Kokbel Pass.

The estimations of the strike-slip rates are summarized in Table 4; not all of them are reliable. Nevertheless, these data show that the slip rates increase along the fault in the north-western direction. They do not exceed 4 mm/a to 4.5 mm/a in segment I, 5 mm/a to 8 mm/a in segment II, and reach approximately 10 mm/a farther to the NE. This may be caused by partial transformation of strike slip in the southeastern part of the fault zone to thrusting on the ENE-trending longitudinal faults of the Central Tian Shan [61,62]. A sharp decline of values and rates from the Late Quaternary movements on the Talas-Fergana Fault to the NW of the Talas range may have been caused by their transformation into displacements on the SW-trending cognate faults of the western flank of Tian Shan [56,63].

Systematic GPS measurements, carried out in Tian Shan since 1992, have not found strike-slip displacements in the Talas-Fergana fault zone and have registered only transverse shortening at a rate of approximately 1 mm/a [64]. Taking into account measurement uncertainties of 1 mm/a to 2 mm/a, Zubovich et al. [63] concluded that the contemporary strike-slip rate on the fault is less than 2 mm/a, which is at a minimum 5 times less than the average Holocene rate of motion on the studied part of the fault zone.

The Tian Shan region of the Talas-Fergana Fault was characterized in the XX century and the beginning of XXI century by its low seismicity. The 22.08.1902 Kashgar, $Ms = 7.8$ and the 02.11.1946 Chatkal, $Ms = 7.5$ earthquakes occurred near terminations of this region, southeastern and north-western, correspondingly, and were related to cognate structures. Characteristic offset magnitudes of topographical features have been identified in segments I and II, while other offset magnitudes are rare or absent (Fig. 11). Similar irregularities in the magnitudes of the strike-slip offsets were found on the dextral San Andreas Fault [12] and on strike-slip faults in Mongolia [65]. This was interpreted as manifestation of pulse displacements during strong earthquakes. The discreteness of offset magnitudes on the Talas-Fergana Fault are probably of the same origin. The differences between adjacent values of lateral offsets, i.e., displacements during individual pulses, vary in segment I from 3 m to 6 m. These differences are 10%–20% more present in segment II, which corresponds to the increase in the average rates of motion, relative to the segment I. Similar lateral offset discreteness is present in the other segments of the fault, but is not so evident.

The last strong earthquakes of the historical epoch were identified in the fault zone by paleoseismological studies [57]. The earliest deposits were dated in structures that were formed or renewed by these seismic events. These dates provided the upper age limit for these events. Two ^{14}C dates in the interval 1419–1444 A.D. were obtained from such deposits in the upper Karakysmak River and the Talas range to the SE of the Karabura Pass, i.e., in the northwestern part of segment VI [59]. The deposits in the Karakulja River source to the NW of the Karakulja Pass (the central part of segment VI) gave dates of 1523–1800 [60]. Several ^{14}C dates were obtained in segment V near the Kokbel Pass [58] and in the upper Karasu River [57]. The majority of the dates demonstrated a dispersion of values from the XVI century to the XVIII century, yet according to the most accurate data, the most probable age of this strong paleoseismic event (Kokbel earthquake) is 1526–1633 (Table 5, Figs. 12 and 13). Spectacular phenomena of two probably seismic-rockfalls dammed the upper Karasu River and formed lakes extending along the fault zone. The fallen sediments of the last third generation are dated to the XIV century by the lichenometric method [66]. Farther to the SE, in the upper Keklikbel River (segment IV), Belousov et al. [66] reported a ^{14}C date of 1317–1405. The deposits, related to the last earthquake, are dated to 1419–1631 in the Jilangach River Basin, segment I [56].

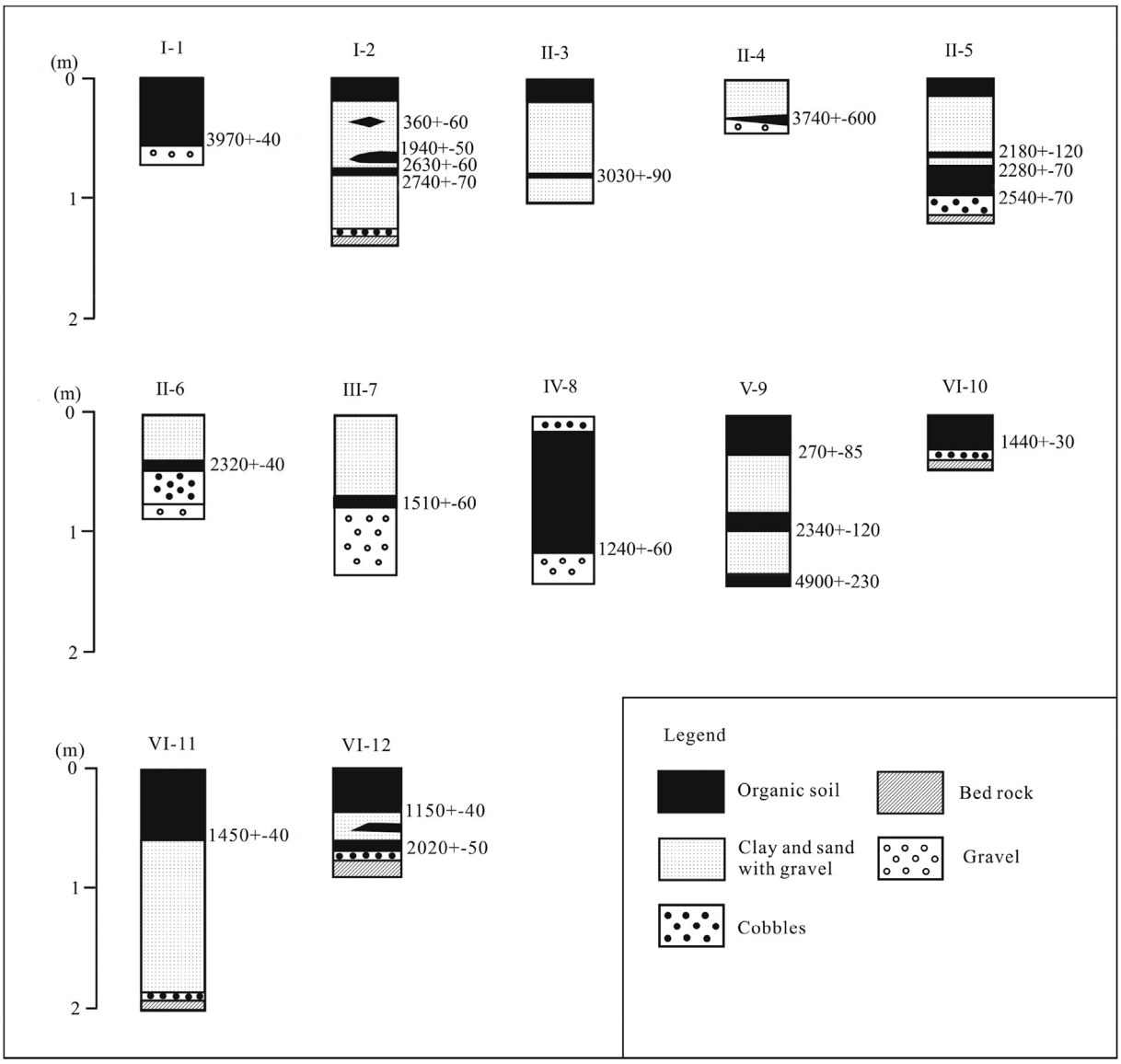

Fig. 10 – Sections of the Late Holocene deposits in different segments of the Talas-Fergana Fault. The 360 ± 60 date in section I-2 is obtained by dating of ceramics. All other dates are obtained by ^{14}C analysis. See text for detailed explanation.

The record of the Kokbel paleoearthquake was found in the approximately 50-km part of segment V. This earthquake occurred in the interval between the second quarter of the XVI century and the first third of the XVII century. The activated fault segment is 50 km–60 km long, which gives a possibility for the estimation of this earthquake's magnitude as Mw approximately 7.1 and an average seismic displacement of approximately 1.1 m–1.2 m [30]. Approximately the same length is characteristic for a part of segment VI that was activated during the earthquake in the Karakulja Pass area. So, the Karakulja paleoearthquake may have the same parameters. The Jilangach paleoearthquake activated, at a as minimum, a 20 km-long section of segment I. This provides a minimum possible magnitude of Mw = 6.6 and an average seismic displacement of several tens of centimeters.

The results of post-seismic deposit dating in the Kokbel Pass, Karakulja Pass, and Jilangach River areas assume that these dates can be attributed to a single seismic event. If this is true, the total length of a seismic rupture could have reached 270 km and an earthquake could have had a magnitude of Mw = 7.9 and an average seismic offset of 6 m. However, disconnection of the mentioned paleoseismic records does not support the idea of single, very strong earthquake.

The records of earlier strong earthquakes are dated to the first half of XV century in the northwestern part of segment VI (the Karabura Pass area) and to the XIV century in segment IV (the Keklikbel River). The latter earthquake could be also expressed by the last generation of rockfall in the upper Karasu River. If the Keklikbel deposits and the rockfall attribute the same earthquake, the total length of its rupture could be > 50 km and the magnitude Mw could be > 7.1.

In spite of inaccuracy in the dating of paleoearthquakes and the estimation of their magnitudes and seismic

Table 4 – The upper and lower strike-slip rate limits in different segments of the Talas-Fergana Fault.

Segment	Lower limit (mm/a)	Upper limit (mm/a)
I	–	4.1–4.4 [53 with correction]
I, NW	–	13–15 (9–11) [56]
II, SE	–	8 – 9 [56] 5.1–8.3 [53 with correction]
II	–	8–9 [56] 9.2–10.3 [53 with correction]
III	~10–15 [53 with correction]	–
IV	2–15 (Q_3^2–Q_4) [53 with correction] 4–6 (Q_2^2–Q_4) [53 with correction]	7.3–11 [5]
V	5.5 – 8.6 (?) [58,59,53 with correction] 4–6 (Q_2^2–Q_4) [55]	–
VI, SE	8–12 (Q_2^2–Q_4) (?) [53 with correction]	9–12 [56]
VI, NW	–	13.4–18.3 [60] ~10 [56]

(Q_3^2 – –Q_4) since the Late Pleistocene glacial till until now; (Q_2^2 – –Q_4) since the Late Middle Pleistocene glacial till until now; all other values are related to the Late Holocene epoch.

displacements, the data are sufficient to suggest that the Tian Shan segments of the Talas-Fergana Fault underwent a series of strong earthquakes in the XIV to XVII centuries and that these earthquakes resulted in a total lateral offset of several meters. We can also assume that the earthquakes and related displacements occurred earlier in the northwestern and southeastern parts of the fault than in the central part. For comparison, strong earthquakes have occurred in the XX century just near the northwestern and southeastern parts of the fault, while the central part has remained quiet.

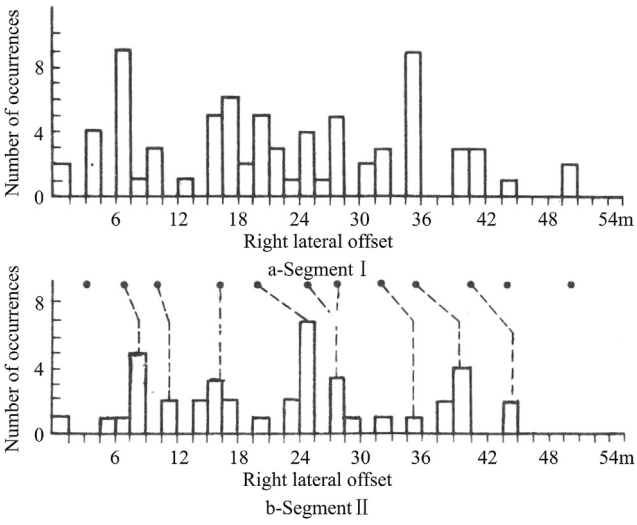

Fig. 11 – Histograms of the Holocene right lateral offsets on the Talas-Fergana Fault [53]. Dots indicate possible earthquake offsets and their correlation between the segments.

4. Active strike-slip faults in fold regions: the epicentral area of the Altai 2003 earthquake in southern Siberia and the Palmyrides in Syria

The major active strike-slip faults that dominate in the neotectonic development and in the recent structure of orogens were analyzed in the previous parts of the paper. Fold regions, where strike-slip faults are important but subordinate structural elements, are examined below, using the examples of the epicentral area of the Altai 2003 earthquake in the Gornyi Altai and the Palmyride fold-thrust belt in Syria.

The Altai 27.09.2003 earthquake with Ms = 7.0 occurred in the fault zone that extends along the southwestern side of the Chuya-Kurai intermountain basin system in the Gornyi Altai [67]. This intermountain basin system consists of the northwestern Kurai and the southeastern Chuya basins, which are separated by the rhombus-like Chagan-Uzun block. Since the Kurai Basin is narrower than the Chuya Basin, the whole system has a triangular form with a sharp angle in the NW (Fig. 14). The basins are filled in with continental Eocene-Quaternary deposits [68–70]. The major active dextral strike-slip Kobdo Fault, with a small reverse component of motion, borders the Chuya-Kurai Basin to the east [62,65]. The Kobdo Fault diverges in the north and its western strand turns to the WNW and borders the Chuya-Kurai Basin to the north. With Quaternary thrusting to the south, associating folding and Late Quaternary dextral offsets are characteristic for this strand. Smaller Late Quaternary offsets have been found in the sides of the Chagan-Uzun block. Dextral and normal fault offsets are characteristic for the southwestern side of the basin. Just the southwestern side was activated during the 2003 earthquake [67].

The epicentral area of the 2003 earthquake was expressed in the land surface by a approximately 65 km-long NW-trending system of seismic ruptures with a dextral displacement of up to 2 m [67]. The dominant majority of the aftershocks formed the 75 km-long and 20 km-wide oval that is elongated at the same direction; the depth of hypocenters is up to 17 km [71]. The mechanisms of the main shock and the strongest (Ms > 6) aftershocks that occurred soon after demonstrate the dextral shift on the NW-trending rupture (Fig. 14). The average displacement in the focus is estimated at 2.5 m [71].

The Institute of Physics of the Earth of the Russian Academy of Sciences established 12 numerical seismic stations in the epicentral area of the 2003 earthquake. They worked from 25.06.2004 until 01.09.2004 and again from 11.08.2005 until 14.09.2005. More than 2000 weak aftershocks were registered during these two sessions. A total of 110 aftershocks with magnitudes <4 were registered by not less than by eight stations, which allowed the possibility to determine nodal planes with sufficient confidence, although the seismic stations were located toward one side of the epicentral area.

The program "FA" was used for the determination of focal mechanisms [72]. The solutions of two aftershock

Table 5 – Radiocarbon-dated ages of soils in the Talas-Fergana Fault Zone.

Locality	Radiocarbon-dated age, years and sample number	Calibrated age, years AD	Information source
1.Karabura	460 ± 40 (SOAN-6524),	1419–1453	[59]
42°10′57″N, 71°39′02″E	405 ± 100 (SOAN-6525),	1429–1633	
	480 ± 35 (SOAN-6527)	1419–1444	
2. Karakuldzha	250 ± 50 (GIN-4299)	1523–1800	[60]
42°05′00″N, 71°55′30″E.			
3. Kokbel	270 ± 85 (SOAN-7021),	1486–1799	[58]
41°42′15″N, 72°52′35″E	370 ± 90 (SOAN-7024)	1447–1633	
	240 ± 50 (SOAN-7026)	1526–1802	
4. Karasu-1	240 ± 50 (SOAN-8143)	1526–1802	[57]
41°39′42″N, 73°02′34″E			
5. Karasu-2	245 ± 65 (SOAN-8141)	1521–1804	[57]
41°39′21″N, 73°03′32″E			
6. Karasu-3	290 ± 60 (SOAN-8139)	1497–1661	[57]
41°37′25″N, 73°07′17″E			
7. Karasu-4	220 ± 80 (SOAN-8144)	1525–1876	[57]
(a) 41°34′54″N, 73°12′12″E	255 ± 70 (SOAN-8145)	1514–1802	
(b) 41°35′09″N, 73°11′49″E	405 ± 50 (SOAN-8146)	1501–1681	
8. Keklikbel	580 ± 30 (GIN-4295)	1317–1407	[66]
41°29′10″N, 73°24′05″E			
9. Dzhilangach	360 ± 60 (GIN-7053)	1459–1631	[56]
40° 53′30″N, 74° 13′00″E			

Note. For the calculation of the radiocarbon-dated age, we used a ^{14}C half-decay period equal to 5570 years. Dating was conducted on the humic acid fraction. Radiocarbon dates are in years from 1950. Calibration and transformation of the radiocarbon dates into calendar dates was conducted using the Radiocarbon calibration program rev 6.1. Standard deviation of the average is 1 s, – with a probability of 68.3%. GIN–Geological Institute RAS (Moscow), SOAN–Institute of Geology and Geophysics RAS (Novosibirsk).

mechanisms, determined from registered signs of P-waves, are shown in Fig. 15a and b. The spatial position of the two nodal planes and the direction of their displacement were determined for each aftershock. Testing of the results was carried out using of the educational computer program of the Moscow State Lomonosov's University [73], which yielded similar results (Fig. 15c, d). As seen in Fig. 15a and c, the position of both nodal planes for the first aftershock were estimated with sufficient confidence. Their position was limited by the data of six stations for the lower plane and by three stations for the upper plane, and vary insignificantly. For the second aftershock, the position of only the lower plane could be estimated with confidence using data from five stations (Fig. 15b, d). The upper (near-vertical) plane could vary 25°–30°; however, its variations were limited by the requirement to be orthogonal relative to the lower plane. This means that the reverse fault remains invariable as the type of focal mechanism. Thus, the testing shows that the parameters of the nodal planes can vary depending on the program used; yet, the type of motion determined remains the same. The solution is well-constrained with respect to motion type.

The mechanisms of the 110 mentioned aftershocks were examined using the described technique (Fig. 16). The mechanisms of the 82 events from 2004 are: 50 (61%) reverse faults, 26 (32%) normal faults, and only 6 (7%) strike-slip faults. The 28 aftershocks of 2005 comprise 18 (64%) reverse faults, 6 (23%) normal faults, and 4 (14%) strike-slip faults [73].

Thus, unlike for the main shock and the strongest aftershocks of 2003, strike-slip mechanisms are rare among the weak aftershocks of 2004–2005 and are present only near the Chagan-Uzun block. The totality of the 2004–2005 aftershock mechanisms cannot be explained as the release of elastic deformation, producing the dextral slip on the NW-trending fault. Instead, they express another stress field that varies over different parts of the epicentral zone [73].

The Palmyrides is the fold-thrust belt that developed in the Miocene and formed finally in the Early Pliocene [22,23]. The folds strike to the NE and the most intense deformation and thrusting takes place in the southern flank of the belt. Some thrusts were activated in the Late Quaternary. The folds are cut by long faults that are convex to the south (Fig. 1). The largest of these are the Jhar and Olab faults that strike to the WNW in the western part, where the Olab Fault is divided to several strands. Both faults demonstrate Late Quaternary dextral and vertical offsets. The Butma-Castal fault zone extends along the northwestern flank of the Palmyrides and demonstrates a record of the Late Quaternary vertical and sinistral offsets, while the Rasafeh–El Faid fault zone continues it. Turning toward the north, the Rasafeh–El Faid fault zone produces significant vertical offsets and deformation of the Quaternary terraces of the Euphrates River [74]. The Butma–Castal–Rasafeh–El Faid fault zone bounds the platformal Aleppo block and separates it from the Palmyrides and the Mesopotamian Foredeep.

Although the majority of the historical earthquakes were related to the DST zone and its associated faults, several strong ($Ms > 6$) historical seismic events were identified in the Palmyrides and the Aleppo block [22,38]. According to the data of the world telemetric seismic network, two strong earthquakes occurred in the Palmyrides during the last time interval: 1994 with $Mw = 5.3$ and 1996 with $Mw = 5.5$. The mechanisms of both earthquakes were interpreted as sinistral slip on the NE-trending faults.

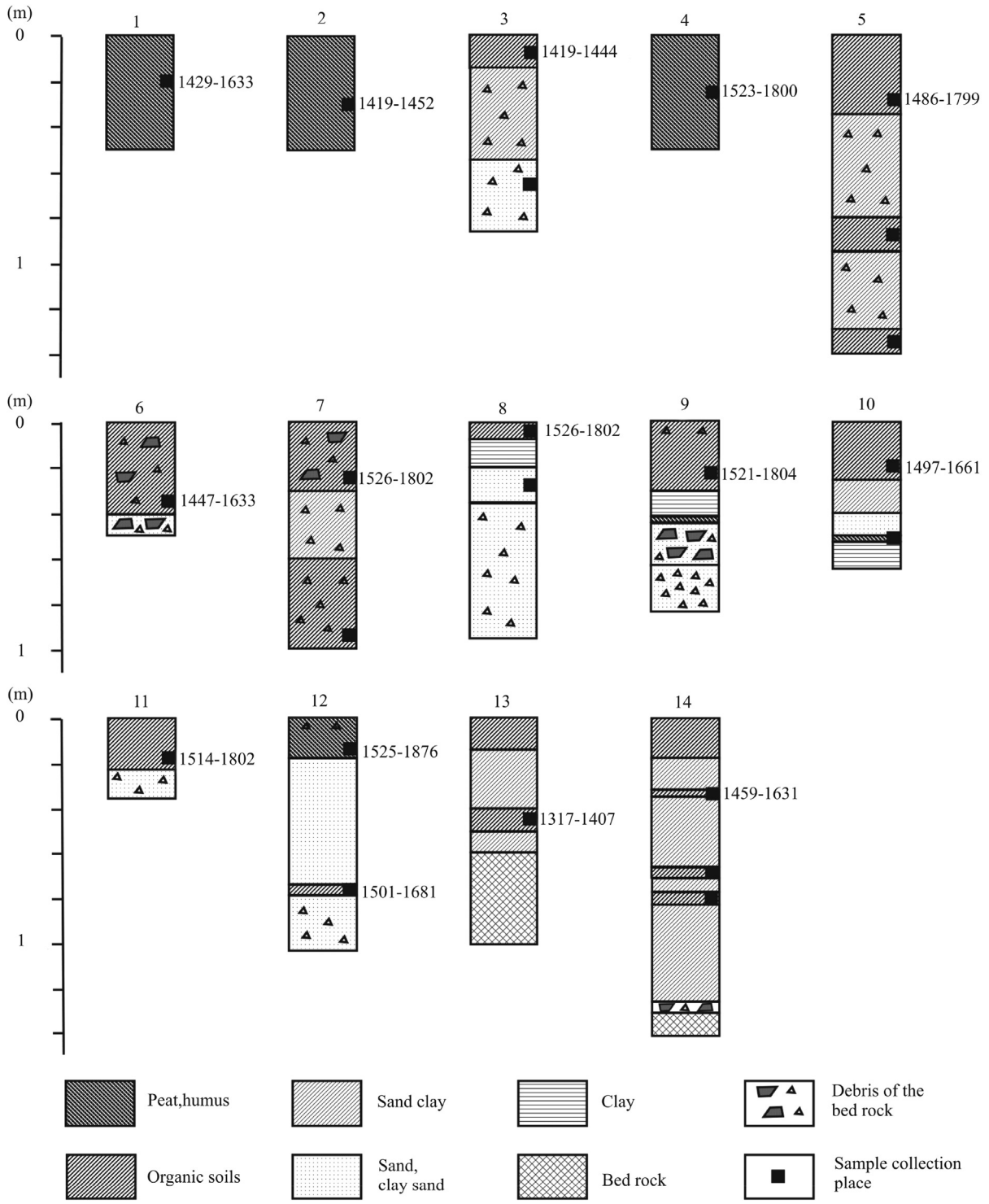

Fig. 12 – Location of samples and calibrated radiocarbon ages, year (numerals in figure) in sections at sites: 1–3, Karabura; 4, Karakuldzha; 5–7, Kokbel; 8, Karasu-1; 9, Karasu-2; 10, Karasu-3; 11, 12, Karasu-4; 13, Keklikbel; and 14, Jilangach [57].

The National seismic network of Syria was founded in 2006. This network registered 292 weak events in 2009–2011. The majority of these events occurred in the DST zone, but a portion happened in the Palmyrides, the Aleppo block, and very rarely in other seismotectonic zones of Syria. Omar et al. [75] selected 50 events in the Palmyrides and the Aleppo block with magnitudes of 1.1–3.3, which were registered, as minimum, by eight seismic stations, and examined their focal mechanisms using of the same technique as was used for the 2004–2005 aftershocks of the Altai 2003 earthquake. The results are distributed as follows: 25 (50%) normal faults, 18 (36%) reverse faults, and only 7 (14%) strike-slip faults

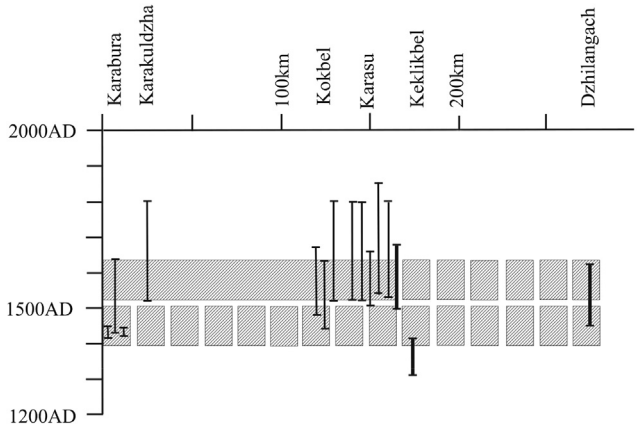

Fig. 13 – Calibrated radiocarbon ages of soil beds in the Talas–Fergana fault zone [57]. Thin and heavy lines are confidence intervals of recent soil and paleosoil ages, respectively.

(Fig. 17). The orientation of the axes of the main normal stress that occurs from these mechanisms varies within the different parts of the region. Only one cluster of 10 events in the west of the Palmyrides conforms to the active fault kinematics and mechanisms of strong earthquakes.

5. Discussion

Two geodynamic peculiarities unite the described active strike-slip fault zones. First, strike slip on the faults occurred mainly during strong earthquakes. Second, during the last decades, when strong earthquakes were absent, the accumulation rate of strike-slip deformation fell in these zones, and the orientation of the axes of elastic deformation differed from the strike-slip ones. This is expressed differently in the described regions.

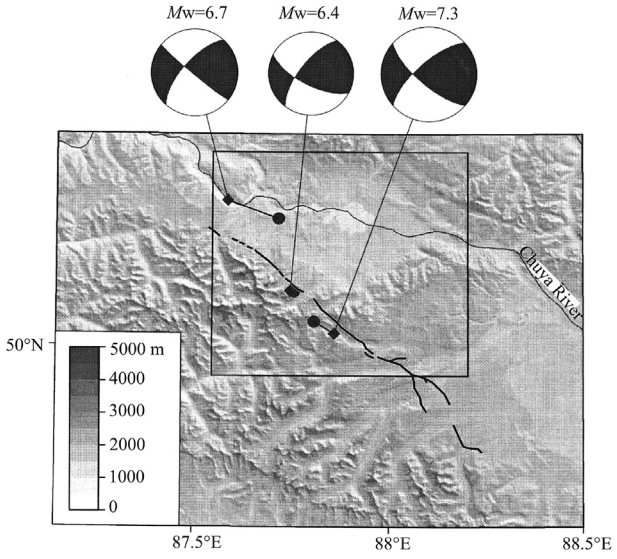

Fig. 14 – Seismic ruptures of the 2003 Altai earthquake [76], as well as the position and focal mechanisms of its main shock and the strongest aftershocks [71]. Black circles show the position of shocks according to the data of the International network and rhombuses show the position of their tensor centroids of the moment.

In the El Ghab segment of the DST, the contemporary accumulation rate of strike-slip deformation is 2–5 times lesser than the average Late Holocene rate. The accumulation rate of the deformation varied, probably, in accordance with variations of seismicity that were expressed by the released seismic energy values. The temporal distribution of the released energy demonstrates a seismic "hyper-cycle" with a ≥1800-year period that combines with 350 ± 50-year seismic cycles. Following the tendency of the "hyper-cycle," the magnitude of a strong earthquake occurring at the peak of the future seismic cycle will not exceed the magnitude of earthquakes that occurred during the previous cycle of the end of the XVIII century–the beginning of the XIX century (Ms = 6.5 to 7.0)–and will not reach an Ms = 7.7 of the 1170 earthquake.

The variation in the accumulation rates of the strike-slip deformation is not a unique peculiarity of the El Ghab segment. We calculated the temporal distribution of the released seismic energy, which was analogous to the calculations carried out for the El Ghab segment, for the adjacent part of the EAFZ to the SE of N39° and E40° [26]. The signs of the seismic cycles with a period of approximately 300 years are present, but they are not expressed as clearly as in the southern and central El Ghab segment (Fig. 4c). This uncertainty may result from the divergence of the Southwestern EAFZ into several strands, which each may have different regimes of development. At the same time, we found more long-term variations, expressed as variability in the released seismic energy values at peak phases of the seismic cycles. These differ from the long-term regularity of the southern and central El Ghab segments. In the Southwestern EAFZ, the values of released energy reach a maximum in the III–VII centuries, with peaks in the III and VI centuries. This is similar to the distribution of seismicity in the adjacent parts of the Alpine-Himalayan Belt, known as the "Byzantine paroxysm" [22,77]. The gradual reduction, with a minimum in the XIV century, and a later rise of the released energy, with a maximum in the XIX century, took place after this. Therefore, the "hyper-cycle" is assumed to also affect the Southwestern EAFZ, but its period (1300–1600 years) and the ages of the phases differ from ones in the southern and central El Ghab segment. The analogous calculation for the northern El Ghab segment yields more uncertain results, as the local earthquakes have had an integral effect on the geodynamic influence of the DST and the EAFZ (Fig. 4b).

The data on the variability of accumulation rates of strike-slip deformation in the Talas-Fergana fault zone is more limited. We only know the average Late-Holocene strike-slip rates and the GPS-measured accumulation rates of deformation for the past two decades. The average Late-Holocene rates are estimated as approximately 10 mm/a in the significantly-studied part of the fault zone and decrease in the SE to 4–4.5 mm/a, as a part of the strike-slip deformation transforms into movements on the conjugate active faults. In general, the

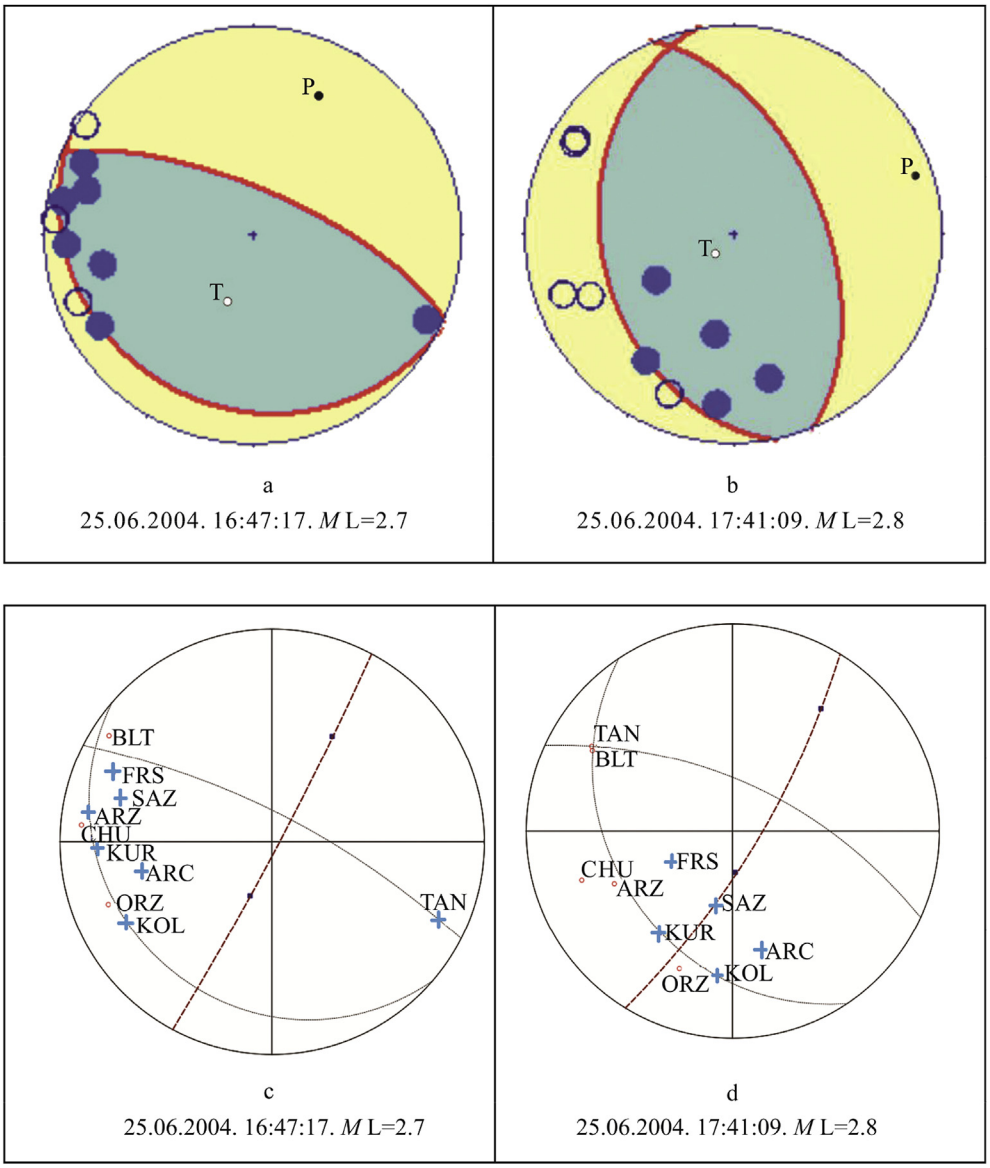

Fig. 15 – Two examples of solutions for the 2004 aftershock mechanisms of the Altai 2003 earthquake from registered the signs of P-wave using the "FA" program [72] (a, b). Light circles are the minus signs and dark circles are the plus signs; T and P are the main axes of extension and compression, respectively. The solutions for the same aftershock mechanisms were calculated using the educational computer program of the Moscow State Lomonosov's University (c, d). Circles are the minus signs and crosses are the plus signs; the thickened dotted line is a plane with main axes of extension and compression [73].

average Late Quaternary slip rates are commensurable to the average strike-slip rate for the whole Quaternary. The contemporary GPS rate is, at a minimum, 5 times less.

The discreteness of the magnitudes of the lateral offsets on the Talas-Fergana fault (Fig. 11) gives a basis to suppose that strike slip occurred mostly during strong earthquakes. The last epoch of strong earthquakes covering the XIV–XVII centuries resulted in several meters of strike slip. The histograms of offsets (Fig. 11) form an illusion of a cyclic recurrence of such epochs of activity. Yet these cycles are imaginary, because with rare exclusions, we do not know the ages of older seismic events. At the same time, the low strike-slip rate at the contemporary phase of low seismicity gives the possibility to assume that the older epochs between the phases of strong seismicity were also characterized by the falling rates of strike-slip deformation.

The analysis of the mechanisms of the weak 2004 and 2005 aftershocks of the strong 2003 Altai earthquake shows a geodynamic situation that differs from the situation of the main shock and its first strong aftershocks. The mechanisms of the main shock and strong aftershocks document the dextral slip on the fault that was confirmed by offsets on seismic ruptures. Tatevossian and Aptekman [78] analyzed the aftershock sequences of the strongest crustal earthquakes of the World

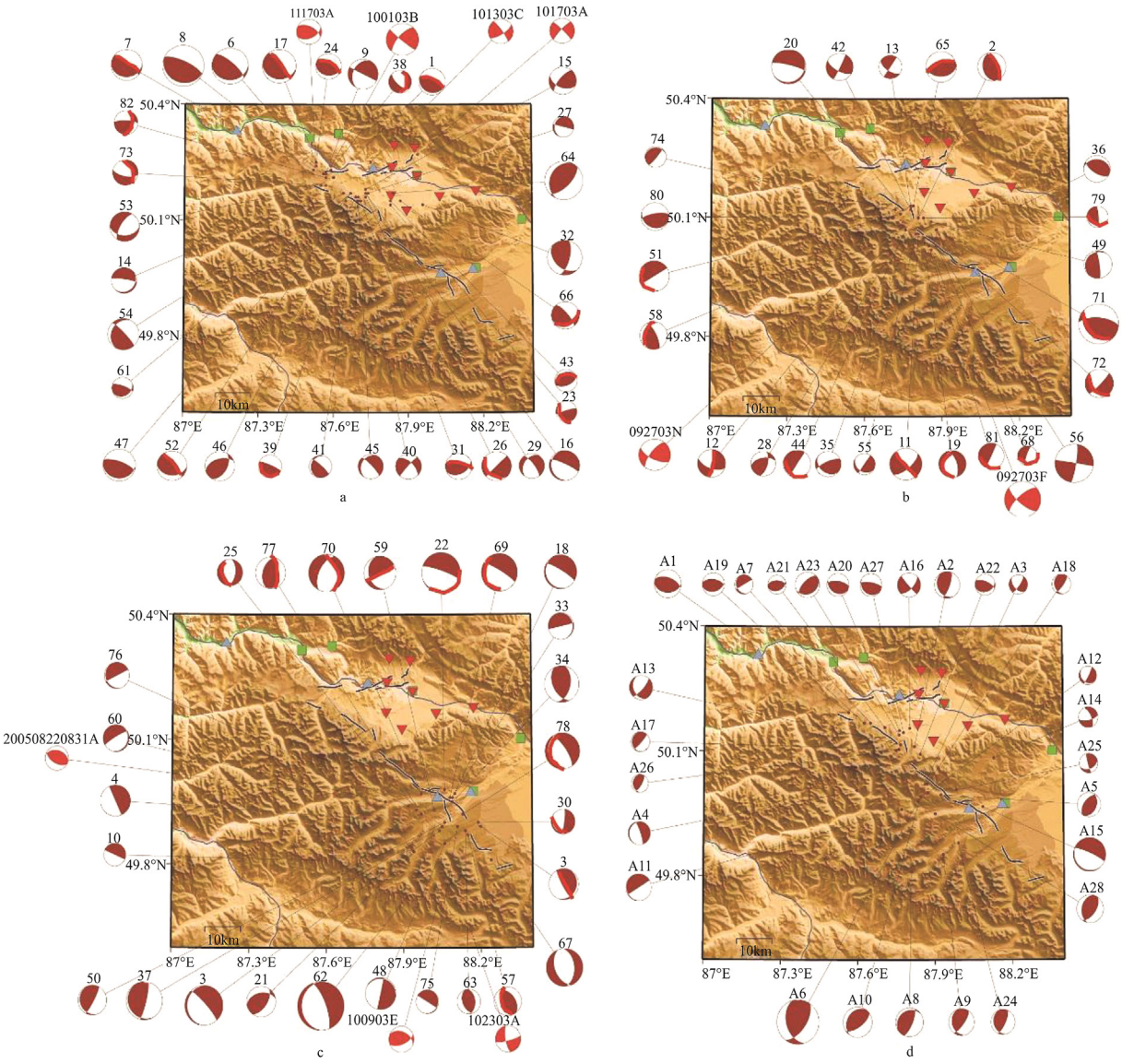

Fig. 16 – Focal mechanism of weak 2004–2005 aftershocks of the 2003 Altai earthquake [73].

and showed that the aftershock focal mechanisms changed over time. Omori's Law is valid only in a short initial interval of aftershock activity. Tatevossian and Aptekman proposed that aftershocks are related initially to the fractures of the seismic zone that preserved their integrity after the rupture in the source of the main shock, and at a later stage they are related to the relaxation of stresses in the medium adjacent to the ruptures. The 2004 and 2005 aftershocks belong to this later stage. The data demonstrate an alternate deformation field than the main shock and initial aftershocks, with a predominance of reverse and normal focal mechanisms. Probably, the accumulated strike-slip deformation was released at that moment. The analysis of the mechanisms of earthquakes in the Palmyrides and the southern Aleppo block, Syria shows also that strike slip is expressed only during strong earthquakes. Strong earthquakes are caused by the general geodynamics in the region, where the Palmyrides are connected with the DST. At other times, the Palmyride seismicity is weak. This reflects a "background" deformation field that is characterized by very small normal and reverse displacements along the minor faults associating with folds.

From the tectonophysical point of view, any tectonic earthquake means that the acting stress exceeds the ultimate strength of the rocks, due to the increase of stress or the decrease of strength. The energy (magnitude) of the earthquake depends on the volume of the rocks, where this limit has been reached and the accumulated stress (elastic deformation) is released. Seismicity changed periodically in many active zones, including the DST and EAFZ, forming several-hundreds-year seismic cycles. The usual explanation for these cycles is that the elastic deformation periodically exceeds the ultimate strength of rocks, and is expressed as a seismic peak. This explanation does not require changes to the rates of

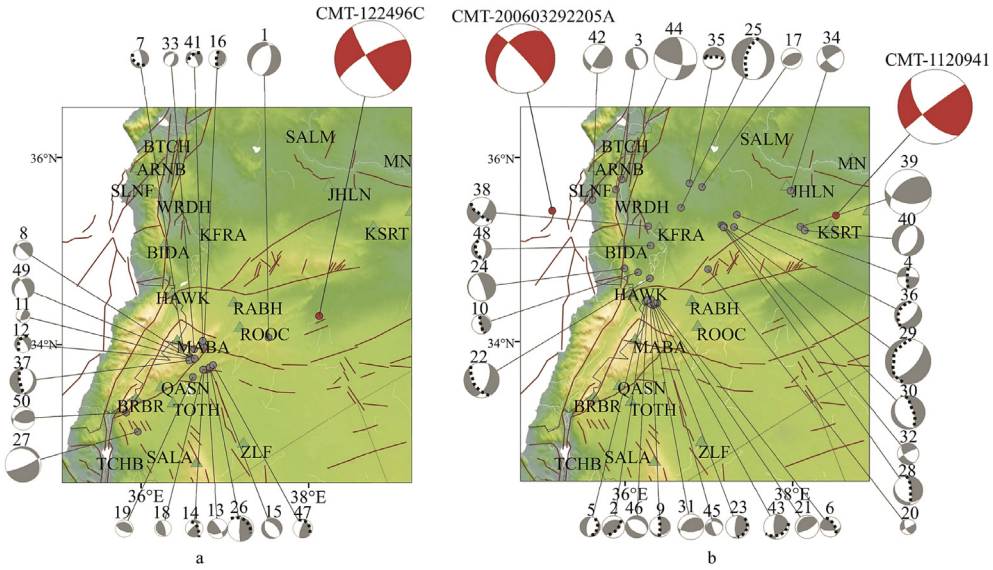

Fig. 17 – Focal mechanisms of the 2009–2011 weak earthquakes in the Western Palmyrides and the southern Aleppo block, Syria [75].

elastic deformation accumulation, i.e., changes to the stress field. The cumulative effect of displacements during individual earthquakes gives the leading contribution to the average fault slip rate, which remains more or less permanent.

The described situations demonstrate that the accumulation rates of strike-slip deformation and, correspondingly, the rates of strike slip on the fault zone have varied over time, up to full interruption. However, these variations are expressed differently. In the El Ghab segment of the DST and the Southwestern EAFZ, they occur with a periodicity of 1300–1800 years that covers the periodicity of the seismic cycles. In the Talas-Fergana fault zone, the epoch of intense seismic strike slip is separated from the present moment of seismic fall and slowing-down of strike-slip deformation accumulation by several centuries. The strike-slip deformation accumulated in the epicentral area of the Altai 2003 earthquake was released during a year and its signs were not manifested until later. The accumulation of strike-slip deformation in the Palmyrides and the release of this deformation during strong earthquakes appear to be episodes in the background of the spatially-changeable stress field. All of this data contradict the thesis of stress field stability in strike-slip zones. Changes to the stress field can occur at different rates, sometimes over months or years. Perhaps, there is a spectrum for these frequency variations.

What are the sources of the described phenomena? It seems doubtful that the source of the increase in seismicity is the reduction of strength. For example, consider an increase in permeability and, correspondingly, in the influence of fluids. Yet, the geological data on fluid regime changes are absent. Furthermore, the accumulation rate of strike-slip deformation would not change in this case. However, it changes together with changes to the seismicity. One could assume that these changes occupy not the deep-seated horizons of the Earth's crust of the strike-slip zone, but only the surficial layers. Their deformation can differ from the deformation of the deep-seated horizons because of different mechanical properties and can results in a detachment. Indeed, GPS measurements characterize only deformation of the land surface. However, another aspect is important. All earthquakes have occurred in the Earth's crust at the described tectonic zones. The depths of the hypocenters of weak earthquakes occurring in the epochs of decreased seismicity and strike-slip movements do not demonstrate systematic differences from the depths of foci of strong earthquakes that have been accompanied by strike-slip displacements. For example, the hypocenters of the 2004 and 2005 weak aftershocks occupied the same depths as the hypocenter of the main shock of the Altai 2003 earthquake [71,73]. The hypocenters of the weak 2009–2011 earthquakes spread in the Palmyrides up to the same depths of 20 km–25 km as the strong 1994 and 1996 earthquakes [75]. Therefore, we are obliged to conclude that the described temporal variations of seismicity and strike-slip rates express, indeed, changes to the rates of strike-slip deformation accumulation and to changes of the stress field in the Earth's crust.

6. Conclusions

There are two types of major active strike-slip fault zones, which differ in their regimes of development. Examples of the first type are the San Andreas and North Anatolian fault zones. In these zones, the rate of strike-slip deformation accumulation was more or less permanent during the Pliocene and Quaternary. These fault zones are not examined in the present study. However, we have studied strike-slip fault zones of the second type. Their peculiarity is in their temporal changes to their accumulation rates of strike-slip deformation. This irregularity is manifested in the El Ghab segment of the DST and in the Talas-Fergana fault zone, where

contemporary (GPS) accumulation of strike-slip deformation is absent or is at a rate several times less than the average rate of strike slip during the Holocene and the longer time intervals (Quaternary or Pliocene-Quaternary). In both zones, no strong earthquakes occurred in the XX century, and GPS measurements only recorded weak transverse shortening. Phases of essential increases in historical seismicity are found in both fault zones. These changes are approximated in the El Ghab zone by a sinusoid that lends the probability to assume a "hyper-cycle" of seismic variations with the period of ≥1800 years. The "hyper-cycle" includes seismic cycles with periods of 350 ± 50 years. The phase of increasing seismicity took place in the Talas-Fergana zone during the XIV–XVII centuries. This seismic pulse could produce the total strike slip of several meters. As the average rate of the Late Holocene strike slip varies in the different segments of the fault from approximately 4 mm/a to 10 mm/a, several such pulses were necessary to create the cumulative Late Holocene offset. We have no data on a periodicity of these pulses.

In the epicentral area of the Altai 27.09.2003 earthquake, the main shock (Ms = 7.0) and the strongest 2003 aftershocks were characterized by the strike-slip mechanisms with the NW-trending plane of the dextral slip. This conformed the seismic rupture that was the approximately 65 km-long NW trending dextral fault with an offset of up to 2 m. The aftershock activity weakened sharply in 2004–2005 and reverse faults and rarer normal faults began to dominate the aftershocks. In the same way, the strong earthquakes of 1994 (Mw = 5.3) and 1996 (Mw = 5.5) in the Palmyrides and the southern Aleppo block in Syria had strike-slip focal mechanisms, while only earthquakes with magnitudes of 1.1–3.3 occurred in the same territory in 2009–2011 and the overwhelming majority had normal and reverse focal mechanisms.

In all mentioned situations, the strike-slip deformation was expressed only or mainly during strong earthquakes. The accumulation rate of deformation diminished during the intervals between these seismic pulses and when the dominant stress conditions led to transverse shortening of the tectonic zone. The question is why these changes to the stress field took place in the DST and the Talas-Fergana Fault, but were not expressed or were expressed more weakly in the San Andreas and North Anatolian fault zones. All of the faults under discussion border major tectonic provinces. The DST, San-Andreas, and North Anatolian faults are the plate boundaries. The Talas-Fergana Fault separates the Western and Central Tian Shan that differ in their Late Cenozoic geodynamic and structural features. However, the kinematic sense of these boundaries is different. The Pacific Plate moves to the NW relative to the North American Plate and the San Andreas Fault manifests this drift. By the same way, the North Anatolian Fault expresses the dextral slip of the Anatolian Plate relative to the Eurasian one. The kinematic sense of the relative plate motion coincides with the slip on the boundary fault in both of these cases.

However, the situation is different in two other cases. The stress field of the El Ghab segment of the DST is characterized not only by the left lateral component that is caused by the drift of the Arabian Plate relative to the African one, but also by the smaller component of transverse compression that is related to the continental slope and is expressed by the transverse shortening of the Coastal range [22]. The latter component becomes appreciable and even dominant locally, when the rate of strike-slip deformation falls. In the same way, not only the right lateral component, but also the smaller component of transverse compression exists in the Talas-Fergana fault zone. The latter component is expressed by the structural signs of transverse shortening of the Fergana and Talas ranges and becomes dominant when the rate of strike-slip deformation falls. The same relationships, but on a localize scale, exist in the epicentral area of the Altai 2003 earthquake and in the western Palmyrides.

The described changes to the accumulation rates of strike-slip deformation and the stress field in the strike-slip fault zones have both practical and theoretical importance. First, they control temporal changes to regional seismicity. If data on these changes are obtained, these must be taken into account for seismic hazard assessment. Second, significant variations of accumulation rates of deformation in fault zones widen the possibility of the tectonophysical interpretation of sources of tectonic events. Events and relationships that are considered impossible within average rates of deformation may be possible at multiple-fold rate increases.

Acknowledgements

This study was supported by the Division of Earth Sciences, Russian Academy of Sciences (6), and the Russian Foundation for Basic Research (14-05-00122). The authors cordially thank Prof. Peter Molnar and Dr. Ruben E. Tatevossian for their useful comments on this manuscript.

REFERENCES

[1] Molnar P, Dayem KE. Major intracontinental strike-slip faults and contrasts in lithospheric strength. Geosphere 2010;6(4):444–467. http://dx.doi.org/10.1130/GES00519.1.
[2] Trifonov VG. Neotectonics of Eurasia. Moscow: Nauchnyi Mir; 1999. 254 p. (in Russian).
[3] Kozacž O, Dolan J, Finkel R, Hartleb R. Late Holocene slip rate for the North Anatolian fault, Turkey, from cosmogenic ^{36}Cl geochronology: implications for the constancy of fault loading and strain release rates. Geology 2007;35:867–870. http://dx.doi.org/10.1130/G23187A.I.
[4] Kozacž O, Dolan J, Finkel RC. A late Holocene slip rate for the central North Anatolian fault, at Tahtakoprü, Turkey, from cosmogenic 10Be geochronology: implications for fault loading and strain release rates. Jour Geophys Res 2009;114. http://dx.doi.org/10.1029/2008JB005760.
[5] Pucci S, De Martini PM, Pantosti D. Preliminary slip rate estimates for the Düzce segment of the North Anatolian fault zone from offset geomorphic markers. Geomorphology 2008;97:538–554. http://dx.doi.org/10.1016/j.geomorph.2007.09.002.
[6] Kiratzi AA. A study of the active crustal deformation of the North and East Anatolian fault zones. Tectonophysics 1993;225(3):191–203.
[7] Trifonov VG. Using active faults for estimating seismic hazard. J Earthq Predict Res 2000;8(2):170–182.
[8] Reilinger R, Barka A. GPS constraints on fault slip rates in the Arabia-Africa-Eurasia plate collision zone: implications for

earthquake recurrence times. Historical and prehistorical earthquakes in the Caucasus. Dordrecht: Kluwer Academic Publication; 1997. p. 91–108.
[9] McClusky SC, Balassanian S, Barka AA, Ergintav S, Georgie I, Gurkan O, et al. Global Positioning System constraints on plate kinematics and dynamics in the Eastern Mediterranean and Caucasus. J Geophys Res 2000;105(B3):5695–5719.
[10] Reilinger R, McClusky S, Vernant Ph, Lawrence Sh, Ergintav S, Cakmak R, et al. GPS constraints on continental deformation in the Africa–Arabia–Eurasia continental collision zone and implications for the dynamics of plate interactions. J Geophys Res 2006;111:Bo5411. http://dx.doi.org/10.1029/2005JB004051.
[11] Allen CR. The tectonic environments of seismically active and inactive areas along the San Andreas fault system. Proceedings of Conference on Geological Problems of San Andreas Fault System. Stanford University Publication. Geological Sciences 1968;11:70–82.
[12] Wallace RE. Notes on stream channels offset by the San Andreas fault, southern Coast Ranges, California. Proceedings of Conference on Geological Problems of San Andreas Fault System. Stanford University Publication. Geological Sciences 1968;11:6–20.
[13] Wallace RE. Earthquake recurrence intervals on the San Andreas Fault. Bull Geol Soc Am 1970;81(10):2875–2890.
[14] Ambraseys NN. Some characteristic features of the North Anatolian fault zone. Tectonophysics 1970;9:143–165.
[15] Walley ChD. A braided strike-slip model for the northern continuation of the Dead Sea Fault and its implications for Levantine tectonics. Tectonophysics 1988;145:63–72.
[16] Westaway R. Kinematic consistency between the Dead Sea Fault Zone and the Neogene and Quaternary left-lateral faulting in SE Turkey. Tectonophysics 2004;391(1–4):203–237.
[17] Daeron M, Benedetti L, Tapponnier P, Sursock A, Finkel RS. Constraints on the post ~25-ka slip rate of the Yammouneh fault (lebanon) using in situ cosmogenic 36Cl dating of offset limestone-clast fans. Earth Planet Sci Lett 2004;227:105–119.
[18] Gomez F, Nemer T, Tabet C, Khawlie M, Meghraoui M, Barazangi M. Strain participating of active transpression within the Lebanese restraining bend of the Dead Sea Fault (Lebanon and SW Syria). In: Cunningham WD, Mann P, editors. Tectonics of Strike-Slip Restraining and Releasing Bends, 290. Geological Society of London Special Publications; 2007. p. 285–303.
[19] Gomez F, Karam G, Khawlie M, McClusky S, Vernant Ph, Peilinger R, et al. Global Positioning System measurements of strain accumulation and slip transfer through the restraining bend along the Dead Sea fault system in Lebanon. Geophys J Int 2007;168:1021–1028.
[20] Ferry M, Megraoui M, Abou Karaki N, Al-Taj M, Amoush H, Al-Dhaisat S, et al. A 48-kyr-long slip rate history of the Jordan Valley segment of the Dead Sea Fault. Earth Planet Sci Lett 2007;260:396–406.
[21] Rukieh M, Trifonov VG, Dodonov AE, Minini H, Ammar O, Ivanova TP, et al. Neotectonic Map of Syria and some aspects of Late Cenozoic evolution of the north-western boundary zone of the Arabian plate. J Geodyn 2005;40:235–256.
[22] Trifonov VG, editor. Neotectonics. Recent geodynamics and seismic hazard assessment of Syria. Moscow: GEOS; 2012. 204 p.
[23] Chorowicz J, Dhont D, Ammar O, Rukieh M, Bilal A. Tectonics of the Pliocene Homs basalts (Syria) and implications for the Dead Sea Fault Zone activity. J Geol Soc Lond 2004;161:1–13.
[24] Gomez F, Khawlie M, Tabet C, Darkal AN, Khair K, Barazangi M. Late Cenozoic uplift along the northern Dead Sea Transform in Lebanon and Syria. Earth Planet Sci Lett 2006;241:913–931.
[25] Trifonov VG, Trubikhin VM, Adjamian J, Jallad Z, El Hair Yu, Ayed H. Levant fault zone in the north-western Syria. Geotectonics 1991;25(2):145–154.
[26] Trifonov VG. Cyclicity of Late Holocene seismicity in the Alpine–Himalayan Belt. Geotectonics 2013;47(6):377–389.
[27] Meghraoui M, Gomez F, Sbeinati R, Van der Woerd J, Mouty M, Darkal AN, et al. Evidence for 830 years of seismic quiescence from palaeoseismology, archaeoseismology and historical seismicity along the Dead Sea fault in Syria. Earth Planet Sci Lett 2003;210:35–52.
[28] Sbeinati MR, Meghraoui M, Suleyman G, Gomez F, Al Najjar H, Al-Ghazzi R. Timing of earthquake ruptures at the Al Harif aqueduct (Dead Sea fault) from archaeoseismology, paleoseismology and tufa cores. In: Intern. Workshop on active Tectonic Studies and Earthquake Hazard assessment in Syria and Neighboring Countries; 2009. p. 78. Abstracts. Damascus.
[29] Wells DL, Coppersmith KJ. New empirical relationship among magnitude, rupture length, rupture width, rupture area, and surface displacement. Bull Seismol Soc Am 1994;84:974–1002.
[30] Ambraseys NN, Melville CP. An analysis of the Eastern Mediterranean earthquake of 20 May 1202. In: Lee W, editor. Historical Seismograms and Earthquakes of the World. San Diego: Academic Press; 1988. p. 181–200.
[31] Trifonov VG, Dodonov AE, Karakhanian AS, Ivanova TP, Bachmanov DM, Ammar O, et al. Seismotectonics of Syria and surrounding areas. In: Intern. Workshop on active Tectonic Studies and Earthquake Hazard assessment in Syria and Neighboring Countries; 2009. p. 76–77. Abstracts. Damascus.
[32] Alchalbi A, Daoud M, Gomez F, McClusky S, Reilinger R, Romeyeh MA, et al. Crustal deformation in northwestern Arabia from GPS measurements in Syria: slow slip rate along the northern Dead Sea Fault. Geophys J Int 2010;180:125–135.
[33] Alchalbi A, Daoud M, Gomez F, McClusky S, Reilinger R, Abu Romeyeh M, et al. Crustal deformation in northwestern Arabia from GPS measurements in Syria: slow slip rate along the northern Dead Sea Fault. In: Intern. Workshop on active Tectonic Studies and Earthquake Hazard assessment in Syria and Neighboring Countries; 2009. p. 23–24. Abstracts, Damascus.
[34] Fedotov SA. On seismic cycle, possibility of quantitative seismic zonation, and long-time seismic prediction. Seismic zonation of the USSR. Moscow: Nauka; 1968. p. 121–150 (in Russian).
[35] Soysal H, Sipahioglu US, Kolcak D, Altdiok Y. Turklye ve cevbesimi tabihsel depbim katalogu. Tuklye biumsel ve teknik arastirma kurumu matematik-fiziki ve biolojik bilimler arastieka grubu. Projeko: TMG 341. 1997. 32 p. (in Turkish).
[36] Archaeoseismololy. In: Stiros S, Jones RE, editors. I.G.M.E. and the British school at Athens, Fitch Laboratory; 1996. p. 268. Occasional paper.
[37] Poirer JP, Taher MA. Historical seismicity in the Near and Middle East, North Africa, and Spain from Arabic documents (VIIth–XVIII centuries). Bull Seismol Soc Am 1980;70(6):2185–2201.
[38] Sbeinati MR, Darawcheh R, Mouty M. The historical earthquakes of Syria: an analysis of large and moderate earthquakes from 1365 B.C. to 1900 A.D. Ann Geophys 2005;48(3):347–435.
[39] Kondorskaya NV, Shebalin NV, editors. New catalog of strong earthquakes in the USSR from ancient times through 1977. Boulder, CO: World Data Center A for Solid Earth Geophysics, NOAA; 1982. 608 p.
[40] Papazachos B, Papazachou C. The earthquakes of Greece. Thessaloniki: Editions Ziti; 1997. 304 p.
[41] Guidoboni E, Comastri A, Traina G. Catalogue of ancient earthquakes in the Mediterranean area up to the 10th century. Rome: Istituto Naazionale di Geofisica; 1994. 504 p.

[42] Plassard J, Kogoj B. Seismisité du Liban: catalogue des séismes ressentis. Collection des Annales-Mémoires de l'Observatoire de Ksara. 3rd ed., t. 4. Beyrouth: Conseil National Libanais de la Recherche Scientifique; 1981. 67 p. Seismologie, cahier 1.
[43] Kondorskaya NV, Ulomov VI, editors. Special catalogue of earthquakes of the Northern Eurasia (SECNE). Zurich: Global Seismic Hazard Assessment Program; 1995. 300 p, http://www.seismo.ethz.ch/gshap/neurasia/nordasiacat.txt.
[44] Tiedemann H. Catalogue of earthquakes and volcanic eruptions. Zurich: Swiss Reinsurance; 1991. 94 p.
[45] Ben-Menahem A. Four thousand Years of Sejsmicity along the dead sea Rift. J Geophys Res 1991;96(B2):20195–20216.
[46] Ambraseys NN, Jackson JA. Faulting associated with historical and recent earthquakes in the Eastern Mediterranean region. Geophys J Int 1998;133(2):390–406.
[47] Ambraseys NN, Barazangi M. The 1759 earthquake in the Bekaa Valley; implication for earthquake hazard assessment in the Eastern Mediterranean region. J Geophys Res 1989;94:4007–4013.
[48] Ambraseys NN, Melville CP. Historical evidence of faulting in Eastern Anatolia and Northern Syria. Ann Geophys 1995;38(3–4):337–343.
[49] Ambraseys NN, Finkel C. The seismicity of Turkey and adjacent areas: a historical review (1500–1800). Istanbul: Muhittin Salih EREN Publication; 1995. 240 p.
[50] Ambraseys NN. Temporary seismic quiescence: SE Turkey. Geophys J 1989;96:311–331.
[51] Taymaz T, Eyidogan H, Jacjsib J. Source parameters of large earthquakes in the East Anatolian fault zone (Turkey). Geophys J Int 1991;106(3):537–550.
[52] Burtman VS. Talas-Fergana strike-slip fault. Moscow: Nauka; 1964. 143 p. (in Russian).
[53] Trifonov VG, Makarov VI, Skobelev SF. The Talas-Fergana active right lateral fault. Ann Tect 1992:224–237. Special Issue, Supplement to Vol. 6.
[54] Dodonov AE. The Quaternary of Middle Asia: stratigraphy, correlation and paleogeography. Moscow: GEOS; 2002. 254 p. (in Russian).
[55] Rantsman EYa, Pshenin GN. Recent horizontal movements of the Earth's crust in the Talas-Fergana Fault Zone from geomorphological analysis data. In: Tectonic movements and recent structures of the Earth's crust. Moscow: Nedra; 1967. p. 155–159 (in Russian).
[56] Burtman VS, Skobelev SF, Molnar P. Late cenozoic slip on the Talas-Fergana Fault, the Tien Shan, Central Asia. Geol Soc Am Bull 1996;108:1004–1021.
[57] Korjenkov AM, Abdieva SV, Burtman VS, Orlova LA, Rust D, Tibaldi A. Evidence of late Medieval earthquakes in the Talas-Fergana fault zone, Tien Shan. Geotectonics 2013;47(6):84–94.
[58] Korjenkov AM, Bobrovskii AV, Mamyrov EM. Evidence for Strong paleoearthquakes along the Talas-Fergana fault near the Kok-Bel Pass, Kyrgyzstan. Geotectonics 2010;44(3):262–270.
[59] Korjenkov A, Rust D, Tibaldi A, Abdieva S. Parameters of the strong paleoearthquakes along the Talas-Fergana Fault, the Kyrgyz Tien-Shan. In: D'amico S, editor. Earthquake Research and analysis – Seismology, Seismotectonics and Earthquake Geology. Rijeka, Croatia: InTech Publishers; 2012. p. 33–84.
[60] Burtman VS, Scobelev SF, Sulerzhitsky LD. The Talas-Fergana fault: recent offsets in the Chatkal district of the Tien Shan. Dokl Acad Nauk SSSR 1987;296(5):1173–1176.
[61] Abdrakhmatov KE, Weldon R, Thompson S, Burbank D, Rubin Ch, Miller M, et al. Onset, style, and current rate of shortening in the central Tien Shan (Kyrgyzstan). Russ Geol Geophys 2001;42(10):1502–1526.
[62] Trifonov VG, Soboleva OV, Trifonov PV, Vostrikov GA. Recent geodynamics of the Alpine-Himalayan collision belt, 541. Moscow: GEOS; 2002. 225 p.
[63] Zubovich AV, Wang X, Scherba YuG, Schelochkov GG, Reilinger R, Reigber Ch, et al. GPS velocity field for the Tien Shan and surrounding regions. Tectonics 2010;29:1–23.
[64] Zubovich AV, Trapeznikov YuA, Bragin VD, Masienko OI, Shchelochkov GG, Rybin AK, et al. Deformation field, Earth's crust structure, and spatial seismicity distribution in the Tien Shan. Russ Geololy Geophys 2001;42(10):1634–1640.
[65] Trifonov VG. Development of active faults. Geotectonics 1985;19(2):95–103.
[66] Belousov TP, Skobelev SF, Strom AL. On estimation of the recurrence period of strong earthquakes of the central Tien Shan (according to data of absolute geochronology). J Earthq Predict Res 1994;3:226–236.
[67] Rogozhin EA, Ovsyuchenko AN, Marakhanov AV, Byrkanov EE, Platonova SG. Tectonic position and geological expressions of the Altai 2003 earthquake. In: Strong 27.09.2003 earthquake in Altai. Proceedings of preliminary study. Moscow: Institute of Physics of the Earth's; 2004. p. 25–37 (in Russian).
[68] Devyatkin EV. Cenozoic deposits and neotectonics in the south-eastern Altai. Moscow: Nauka; 1965. 242 p. (in Russian).
[69] Zykin VS, Kazansky AY. Main problems of stratigraphy and paleomagnetism of Cenozoic (Prequaternary) deposits of Chuya depression of Gorny Altay. Russ Geololy Geophys 1995;35:75–90.
[70] Zykin VS, Kazansky AY. New data on Cenozoic deposits in the Chuya depression, Gorny Altai: stratigraphy, paleomagnetism, evolution, continental rift tectonics and evolution of sedimentary basins. Novosibirsk: Russian Academy of Sciences; 1996. p. 74–75.
[71] Arefiev SS, Aptekman ZhYa, Bykova VV, Matveev IV, Mikhin AG, Molotkov SG, et al. The source and aftershocks of the Altai (Chuya) earthquake of 2003. Izvestiya. Phys Solid Earth 2006;42(2):167–177.
[72] Collection of programs for determination of focal mechanisms of earthquakes and their graphic presentation. In: Report on complex seismological and geophysical studies in Kamchatka and Komandor Islands (01.01.2003-31.12.2003). Petropavlovsk-Kamchatsky: RAS, Geophysical Survey, Kamchatka Experimental-Methodological Seismological Group; 2004 (in Russian).
[73] Omar KhM, Aref'ev SS, Rebetsky YuL. Mechanisms of 2004-2005 aftershocks and stress parameters in the focal area of the Altai 2003 earthquake. Geophys Res 2012;13(3):56–73 (in Russian).
[74] Trifonov VG, Bachmanov DM, Ali O, Dodonov AE, Ivanova TP, Syas'ko AA, et al. Cenozoic tectonics and evolution of the Euphrates valley in Syria. In: Robertson AHF, Parlak O, Ünlügeng UC, editors. Geological Development of Anatolia and the Eastmost Mediterranean Region, vol. 372. London: Geological Society; 2012. http://dx.doi.org/10.1144/SP372.4. Special Publications.
[75] Omar KhM, Tatevosyan RE, Rebetsky YuL. Mechanisms of earthquakes and stress parameters of the Earth's crust in Syria. Bulletin of Kamchatka Regional Association "Education-Scientific Center". Earth Sci 2012;20(2):231–240 (in Russian).
[76] Rogozhin EA, Ovsyuchenko AN, Marakhanov AV, Ushanova EA. Tectonic setting and geological manifestations of the 2003 Altai earthquake. Geotectonics 2007;41(2).
[77] Trifonov VG. Tectonic and climatic rhythms and the Development of Society. In: Florinsky I, editor. Man and the

Geosphere. N.-Y.: Nova Science Publishers, Inc; 2010. p. 257–305.

[78] Tatevossian RE, Aptekman ZhYa. Aftershock sequences of the strongest earthquakes of the World: stages of development. Izvestiya, Phys Solid Earth 2008;44(12):945–964. http://dx.doi.org/10.1134/S106935130812001X.

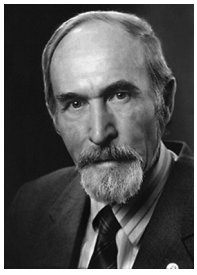

Trifonov, Vladimir G., Professor, Dr. Sci., Senior scientist of the Geological Institute of the Russian Academy of Sciences, Moscow, the (co)author of 225 books and papers. He is a well known specialist in general tectonics and geodynamics, neotectonics, seismotectonics, active faulting, recent geodynamics, and these fields have great influence on human life and safety. He was also a co-chairman of the Project II-2 "World Map of Major Active Faults" of the International Lithosphere Program.

Korzhenkov, Andrey M., Head of Laboratory, Schmidt's Institute of Physics of the Earth, Russian Academy of Sciences, the (co)author of more then 270 scientific publications. He has got his PH.D. majored in Geological and Mineralogical Sciences, supervised by Prof. Dr. Habil. Oleg K. Chediya, from Institute of Seismology, in 1988. He has been awarded Alexander Von Humboldt Foundation research fellowship from Potsdam University, Germany during 2000–2002 and letter of commendation from President of National Academy of Sciences of Kyrgyz Republic in 2007. His Areas of Expertise includes Archeoseismology, active tectonics, tectonic geomorphology; Neotectonics, fault zone structure and geomorphology; earthquake surface rupture and paleoseismology; fault zone structure and paleoseismology in the Tien Shan, Middle East and Caucasus mountains; active deformation in central Asia; integrated investigation of earthquake hazards; and Quaternary and Cenozoic Geology.